P-081 Microwave heating of liquid crystals under *in-situ* microwave irradiation solid-state NMR

Yugo Tasei[1], Teruyuki Fujito[2], Izuru Kawamura[1] and Akira Naito[1]
[1]Graduate School of Engineering, Yokohama National University
[2]Prove Laboratory Inc.

We have developed an *in-situ* microwave irradiation solid-state NMR apparatus. In the NMR probe, microwave coil is wound inside the radio wave coil, and microwave and radio wave frequency are doubly tuned. Using this probe NMR signals can be measured under the microwave irradiation condition. ^{1}H NMR signals of liquid crystal sample, 4-(trans-4-amylcyclohexyl)benzonitrile whose melting point is 55˚C, were successfully measured under microwave irradiation condition. The results indicated that the spectra under the microwave irradiation at 30˚C appeared as those in the signal in the isotropic phase, while it was noted that they are different from those without microwave irradiation at 56.5˚C.

【Introduction】In recent years, microwave heating is used extensively in the activation of organic reaction as well as activity enhancement of the enzymes. However, molecular mechanism of microwave effect on the chemical reaction has not well understood yet. On the other hand, chance of exposing with microwave is now increasing by the use of mobile phone, satellite broadcasting, and wireless LAN. Although, the microwave effect of our body has not well characterized yet, it is important to evaluate how exposures with the microwave affect to our body. To this end, we have developed an *in-situ* microwave irradiation solid-state NMR apparatus to reveal the microwave to the material and the biological molecules

【Experimental】

In-situ microwave irradiation solid-state NMR The apparatus was modified based on the originally developed Microwave heating 2D NMR spectroscopy (Fig.1) [1, 2]. In the NMR probe, microwave coil is wound inside the radio wave coil, and microwave and radio wave frequency are doubly tuned. The microwave circuit is tuned properly to 2.45 GHz by using a sweep generator. NMR spectra were recorded on a Chemagnetics (Fort Collins, CO) CMX-400 Infinity NMR spectrometer, equipped with a microwave transmitter (IDX, Tokyo Electric Co. Lid.) which is capable of transmitting 1.3kW pulsed sample. In this system, microwave was completely isolated from radio wave, so that NMR signal can be observed under microwave irradiation.

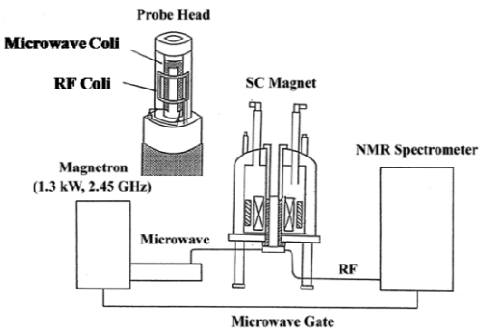

Fig.1 Block diagram of the microwave heating NMR spectrometer equipped with a microwave transmitter. Microwave and radio wave coils in the probe head are also shown.

Solid-state NMR measurements ^{1}H NMR spectra using the 90^o pulse of 4 μs and the recycle time of 2 s were measured for liquid crystal sample, 4-(trans-4-amylcyclohexyl)benzonitrile (Fig.2), whose melting point is 55˚C. Using microwave irradiation probe, NMR signals can be measured under two conditions which are under constant temperature and microwave irradiation conditions. The former spectra were acquired after waiting for 30 minute at various temperatures. The later were measured under microwave irradiation continuing at 30^{o}C

Microwave irradiation, Liquid crystal, Solid-state NMR

【Result and discussion】

Figure 3 shows spectra in the thermal heating (a) (b) and microwave irradiation (c) (d) (e) (f). We have successfully observed ^{1}H NMR signals of liquid crystalline sample under continuous microwave irradiation (Fig.3 (c) (d) (e) (f)). The results indicated that the isotropic phase appeared in the spectra under microwave irradiation at 30˚C after 352s since microwave irradiation turned on. The thermal heating spectrum at 56.3^{o}C (Fig.3 (a)) corresponds to that after 408 s (Fig.3 (e)). It was noted that microwave irradiation spectra (Fig.3 (c) (d) (e)) did not show completely the same line shape as the thermal heating spectra, but show a little narrow spectra. After sample changed from liquid crystalline to isotropic phase, spectra under microwave irradiation did not show the same pattern. These observations indicate that liquid crystalline molecule under microwave irradiation shows microwave heating state. In the microwave thermal heating state, it is suggested that the molecules are more mobile as compared to the thermally heating state.

It was demonstrated to discriminate between heating and microwave irradiation conditions by *in-situ* microwave irradiation solid-state NMR.

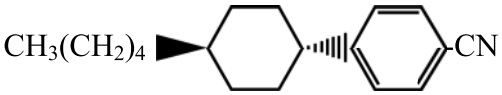

Fig.2 Structure of 4-(trans-4-amylcyclohexyl)benzonitrile

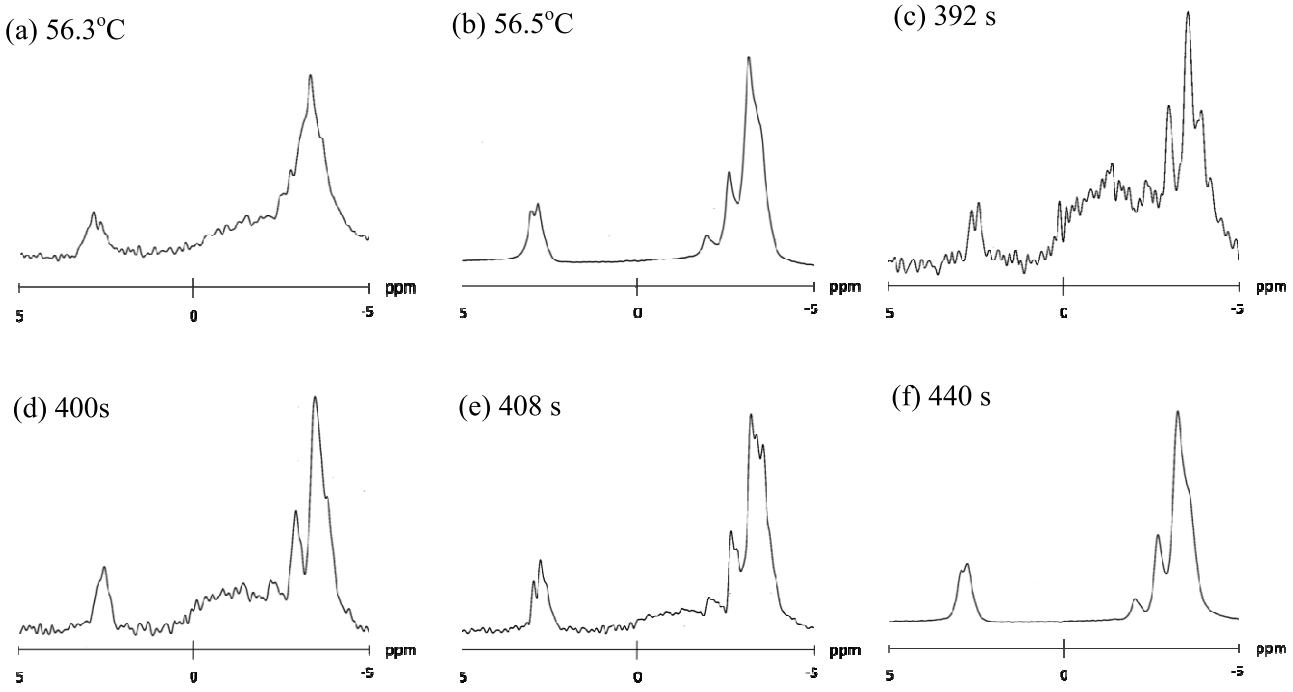

Fig.3 ^{1}H NMR spectrum without microwave irradiation (a) 56.3^{o}C, (b) 56.5^{o}C, with microwave irradiation after (c) 392 s, (d) 400 s, (e) 408 s, (f) 440 s since microwave irradiation turned on.

References

[1] A. Naito et al, Thermotropic Liquid Crystals (2007), 85-116 *Springer*.
[2] A.Naito et al, Materials Science & Technology (2010) 2886-2894

P-082 Improvement of X_0 shim coil

Tatsuya Matsunaga[1, 3], Takashi Mizuno[2], and K. Takegoshi[1]

[1]Division of Chemistry, Graduate School of Science, Kyoto University,
[2]JEOL Resonance Inc. and [3] Global COE.

An X_0 shim coil is a device for precise adjustment of the magic angle in solid-state NMR. By controlling the current for the X_0 shim coil, one can realize the precision of the angle adjustment of 0.001 degree order. In this work, we deal with practical problems associated with the coil.

Introduction

Magic angle spinning (MAS) is a standard method to realize high resolution in solid-state NMR. In MAS, it is essential to adjust the sample spinning angle θ to the magic angle $\theta_M = \cos^{-1}\frac{1}{\sqrt{3}} \sim 54.71°$. For example, in natural-abundance ^{2}H MAS NMR, one has to adjust the angle within the error of 0.03° [1], and furthermore, in ^{27}Al STMAS NMR, angle maladjustment exceeding 0.008° degrades the spectrum [2].

So far, a typical way of the adjustment has been manual rotation of the shaft. Hence, it is hard to adjust the angle precisely and reproducibly. Recently, we propose an idea of tilting the magnetic field instead of the spinning axis [3]. For this purpose, we developed an X_0 shim coil, which produces an additional static field B_x perpendicular to the main field B_0 to tilt the net field B_{eff} from B_0. By controlling the current, the magic angle can be adjusted within an error less than 0.001° using a high precision constant-current power supply. Though the X_0 shim coil was developed for a cryocoil MAS probe [4], which does not have the angle-adjustment mechanism, it can also be used to work with various commercial MAS probes, attached to the probe like an rf shield.

It is, however, fain to point out that the X_0 shim coil has the following practical problems; (1) spectral broadening due to the inhomogeneity of the magnetic field of the X_0 shim coil, (2) mechanical tilting of the probe due to the Lorentz force, and (3) heating caused by the current. In this work, we report our recent progress toward solution of these problems.

Fig. 1 Pictures of X_0 shim coils.
Left; the 2nd prototype: coil size ϕ71 mm × 90 mm.
Right; the 3rd prototype: coil size ϕ72 mm × 172 mm.

Problems and solutions

(1) In the previous X_0 shim coil which we call the 2nd prototype [3] (Fig. 1 left), the field homogeneity was not satisfactory. Accordingly, we have revised the design of

Keywords; MAS, infinitesimal adjustment, solid-state NMR

the X_0 shim coil, and built the 3rd prototype (Fig.1 right), in which the height of the coil is twice that of the 2nd prototype. In order to examine its performance, we measured ^{13}C CP MAS NMR of adamantane using a 4 mm MAS probe doubly tuned at 300 and 75 MHz with the X_0 shim coil operating at the current designated in Figure 2.

We found that, in the 3rd prototype, the $^{13}CH_2$ line width increased from 2.2 Hz to only 3.8 Hz with the currents of up to 10 A. The current of 10 A corresponds to the tilting of the static magnetic field of 7 T by 0.05°. Even in the solid state, the adamantane molecules are tumbling considerably at room temperature, eliminating ^{13}C chemical shift anisotropy (CAS). It follows that the width of the ^{13}C resonance line is solely determined by the homogeneity of the net field. In addition, because the ^{13}C line width of adamantane is much less than an ordinary ^{13}C line width in MAS NMR, the increase of the line width in Fig. 2 (a), 1.6 Hz ~ 0.02 ppm, is ignorable for the ordinary ^{13}C line width. Hence this result shows that we can adjust the deviation of the angle ± 0.05° without introducing appreciable line broadening.

(2) The magnetic field of the X_0 shim coil increases the strength of the net field $B_{eff} = \sqrt{B_0^2 + B_x^2}$. The calculated shift of the peak position is ca. 23 Hz with the current of 10 A. However, we observed a much larger shift, as shown in Fig.2 (b). This is ascribed to the Lorentz force acting on the X_0 shim coil, tilting the body of the probe. From the ^{13}C peak shift, the probe orientation was estimated to change by ± 1° with the current of ± 10 A. At present, we are preparing a device to fix the probe with the main magnet. Results will be shown in the venue.

(3) The current through the X_0 shim coil also causes heating, which may damage the sample and the probe. Indeed, the power of as large as ca. 60 W is consumed with the current of 10 A. Accordingly, we attached heat dissipation plates on the X_0 shim coil and blew dry air from the bottom to the top. It improved the problem dramatically.

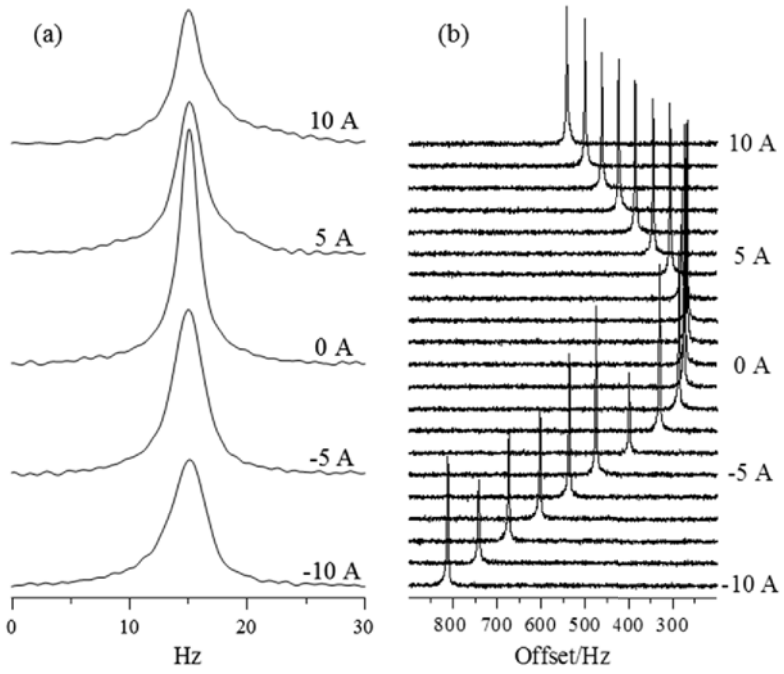

Fig.2 ^{13}C CP MAS NMR spectra of adamantine for various currents applied to the X_0 shim coil; (a) shapes of the $^{13}CH_2$ peaks and (b) offsets of these peaks from the carrier frequency. The spinning frequency is 10 kHz and the decouple frequency is 47 kHz.

Acknowledgement

This study was financially supported by SENTAN/JST (the adoption in 2010) and T. Matsunaga was supported by research fellowship of Global COE program.

Reference

[1] T. Mizuno et al., J. Am. Chem. Soc., 128 (2006) 9683.
[2] C. Huguenard et al., J. Mag. Res. 156 (2002) 137.
[3] T. Mizuno et al., the 48th Annual Meeting of the Nuclear Magnetic Resonance Society of Japan, P058.
[4] T. Mizuno et al., Rev. Sci. Instrum. 79 (2008) 044706.

P-083 Sensitivity enhancement of ^{33}S-MASNMR using cryocoil MAS probe

Shinji Matsuo[1], Takashi Mizuno[2], Yasuto Noda[1]and K.Takegoshi[1]

[1]Graduate school of Science, Kyoto University
[2]JEOL RESONANCE Inc

ABSTRACT

Sulfur is included in a wide variety of organic and inorganic materials, and it plays an important role. However, there are a few solid-state ^{33}S NMR studies because of the demerits such as small gyromagnetic ratio, low natural abundance (0.76%), and broadening due to quadrupolar interactions. Here, we report high resolution solid-state ^{33}S NMR by using a cryocoil MAS probe, which can improve the sensitivity by 3 to 4 times compared to the conventional MAS probes.

INTRODUCTION

Sulfur is present in a wide variety of organic and inorganic materials, as well as biologically important molecules. Many sulfur-containing materials are of industrial and technological importance. However, solid-state ^{33}S NMR has not been popular, because of its low sensitivity due to its low gyromagnetic ratio (γ=2.055×10^7 radT^{-1}s^{-1}), low natural abundance (0.76%), and broadening due to quadrupolar interactions. In this work, we study ^{33}S MAS NMR using a cryocoil MAS probe. In this detection system, the coil and the preamplifier are cooled below 30 K, while the spinnig sample can be kept at room temperature. In cryocoil ^{1}H MAS NMR, the sensitivity was enhanced by a factor of 4 [1]. Here, we report on sensitivity enhancement of the ^{33}S signals.

EXPERIMENT

In this work, we used our second prototype of the cryocoil MAS probe equipped with a chemagnetics 5mm spinning system. The coil was tuned at 45~48 MHz. First, we calibrated the rf pulses by deuterium NMR using deuterated chloroform in a 4 mm glass tube. The deuterium NMR experiment was performed at 46.261 MHz in a 7 T wide-bore magnet. In this experiment, we cooled only the coil to 15 K and the preamplifier was kept at room temperature . Then, we measured ^{33}S MAS NMR in CaS in 14.1 T under sample spinning at 5 kHz. The amount of the sample was 90 mg, and the ^{33}S carrier frequency was 46.066MHz.

Figure1:A photograph of the second prototype of cryocoil MAS probe

RESULTS

Figure 2(a) and (b) shows ^{2}H spectra of deuterated chloroform obtained with coil temperatures of 300 K and 15 K. In both cases, the preamplifier was at room temperature. By cooling the coil, signal-to-noise ratio (S/N) was enhanced by a factor of 2.2. We found that the gain in the Q factor of

cryocoil, ^{33}S, sensitivity enhancement

the S/N depends not only on the coil temperature (T_C), but also on the temperature (T_a) of the preamplifier. According to REFERENCE [1], S/N is proportional to $[(Q)/(T_C + T_a)]^{1/2}$, from which the expected gain in the sensitivity is calculated to be 2.9. The experiment result is close to a theoretical value. Further gain in the sensitivity is expected by cooling the preamplifier as well.
Figure 3 shows a preliminary result of ^{33}S MAS NMR in CaS obtained without coil and preamplifier cooling. Currently, ^{33}S MAS NMR experiment with the cryogenic coil and preamplifier is in progress. Results will be presented in the poster. And then we aim at investigation into organic materials with sulfur such as cysteine and methionine.

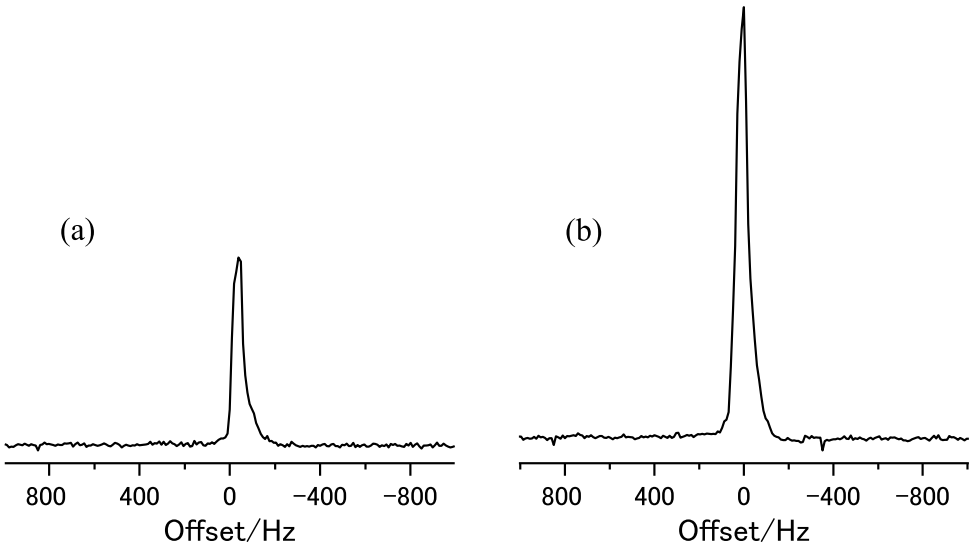

Figure2: Comparison of S/N by second prototype of the cryocoil MAS probe. Deuterium NMR by single pulse. Sample: deuterium chloroform. (a): Coil temperature=298K, Q factor=80, 90° pulse width=6.9 μs (input 184 W), 10 scans. (b): Coil temperature=15 K, Q factor=383, 90° pulse width=6.0 μs (input 184 W), 10 scans.

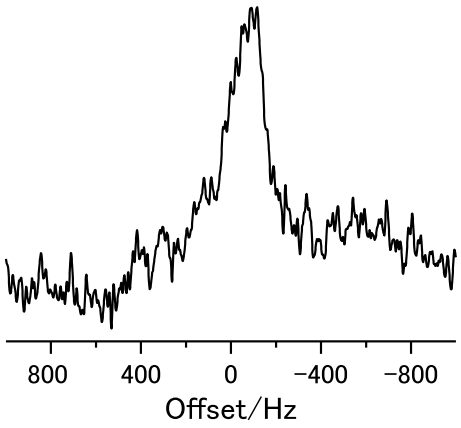

Figure3: ^{33}S MAS NMR spectrum of CaS by second prototype of the cryocoil MAS probe. Sample: CaS. Spinning speed=5 kHz. Detection system temperature=298 K, 90° pulse width=7.0 μs (input 165 W), 5000 scans with 10 Hz lime broadening, center frequency=46.04 MHz, experiment time was 15 h.

REFERENCE

[1] T.Mizuno et al., Rev. Sci. Instrum. 79 (2008) 044706, T.Mizuno et al., Rev.Sci.Instrum.80 (2009) 124702

ACKNOWLEDGEMENT

This study was financially supported by SENTAN/JST (the adoption in 2010).

P-084
Y

Evaluation of cellulose degradation properties in microbial ecosystem by solution and solid-state NMR

Keiko Okushita[1], Tomohiro Iikura[1], Yasuhiro Date[2], Yoshiyuki Ogata[2], Eisuke Chikayama[1,2], and Jun Kikuchi[1,2,3,4]

[1]Grad. Sch. of Nanobio., Yokohama City Univ., [2]RIKEN Plant Sci. Cent.,[3]Biomass Eng. Prog., RIKEN Clust. Inov., [4]Grad. Sch. of Bioagri., Nagoya Univ.

ABSTRACT

Cellulose is consisted the most in biomasses on the earth and expected to be converted, that is, efficiently degraded to “sugar platform” as energy source and feedstock of the raw materials. For the construction of the efficient and continuous energy supply system by biomass, we need to understand the degradation process in detail and choose the way to process the biomass. In this presentation, we will show the example of the analytical method for the evaluation of ^{13}C labeled cellulose degradation in microflora of methane fermentation bacteria by the data mining of both NMR spectra and DNA sequences by statistical calculations.

INTRODUCTION

From the limit of residual fossil fuels, new style of energy supply is demanded. As one of plans, the energy supply by biomass degradation (such as biofuel) is suggested and the study field is expanding. Especially, cellulose degradation study is important because it is the most abundant biomass on the earth. Considering the construction of energy supply system based on cellulose in biomass, the choice of enzyme would be important because the cellulose degrading enzyme, cellullase is bottleneck of its cost down in general. Methane fermentation flora is known to contain many kinds of cellulase. Therefore it would be a suitable approach for the choice of enzyme that the degradation property information (Meta-metabolome, etc.) and the result of the Meta-genome analysis in microbial flora can be correlated by statistical analysis.

Our concept and strategy for the investigation of cellulose degradation property in methane fermentation sludge are shown in Fig. 1. The data of biomass, metabolites and DNAs corrected by ^{13}C CP/MAS, solution NMR and DNA sequencer respectively would be assembled as data matrices. DNA sequence data can be analyzed by our original tool E-class[1]. Using the data matrix, correlation analysis would be carried out such as NMR spectra and DNA sequences. For statistical analysis like correlation, many amounts and kinds of data are necessary. NMR is the nondestructive method to analyze samples, and in the analysis of organic samples, ^{13}C signals can be detected selectively from environmental complexity. In addition, various kinds of information can be extracted from NMR data of proper pulse sequence experiments. Therefore, NMR experiments with ^{13}C labeled sample make it possible selective analysis for the degradation behavior in the complex microflora environment. Therefore, we introduce solution and solid state NMR results of ^{13}C labeled cellulose degradation in microbial flora of methane fermentation bacteria in this study.

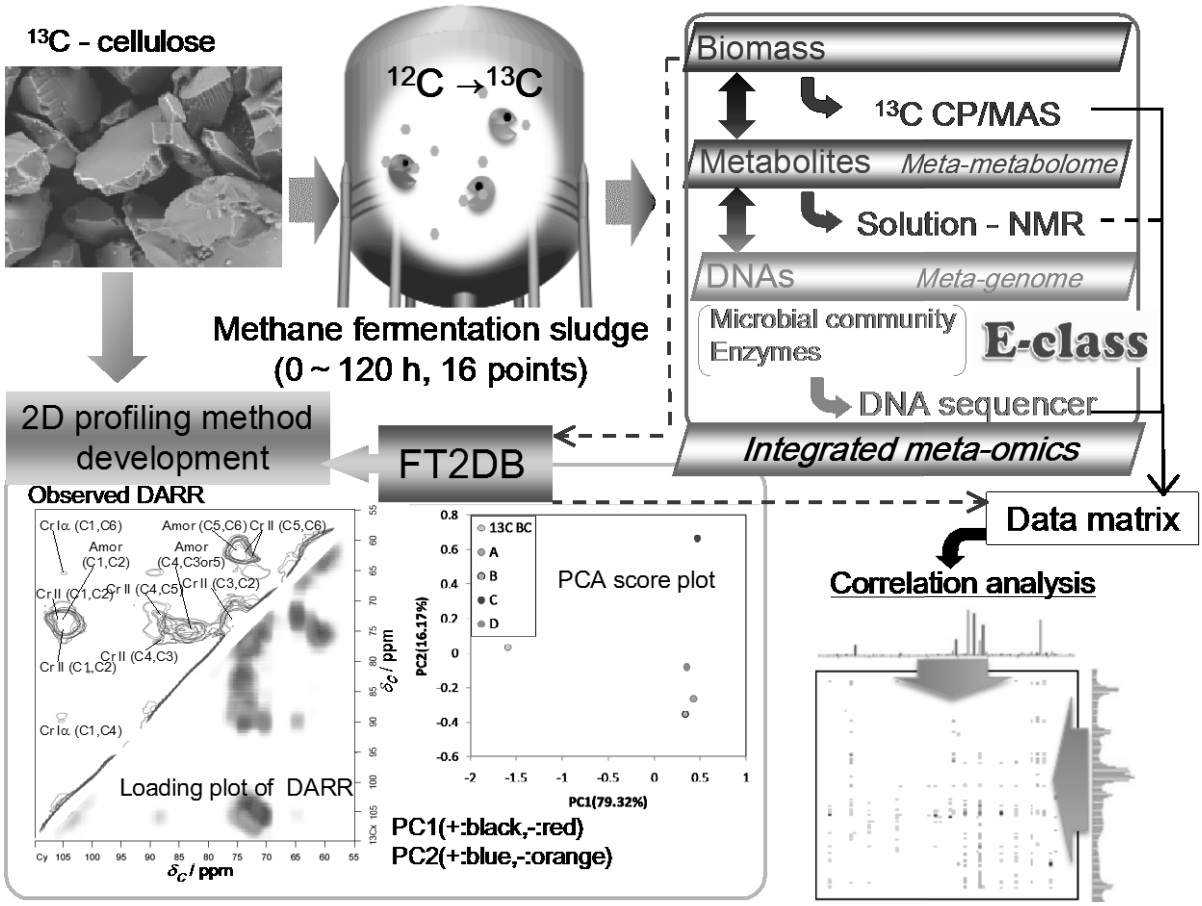

Fig. 1 Concept and strategy of our project. We are mining for the bacteria or enzyme that can degrade cellulose effectively. As one of the method to provide the useful information for specifying the class of bacteria or enzyme, the development of NMR techniques and profiling method takes important part for obtaining data matrices with 2D-NMR spectral binning[2,3].

EXPERIMENTS

・Sample preparation

[Samples for the investigation of analytical method]

Film pieces of ^{13}C-labeled or ^{12}C- bacterial cellulose (10 mg) produced by *Acetobacter xylinum* were dissolved in each ionic liquid (1 g) heated to 120 ºC. After 30 min. incubation for dissolution, 2 ml of pure water was added into each solution for regenerating cellulose and mixed by vortex mixer. Regenerated cellulose mixture was filtered and washed by pure water 10 times, and then dried in vacuum for 6 hours at room temperature. Ionic liquids used to modify cellulose structure were EmimAc (A), BmimAc (B), EmimCl (C), and EmimDEP (D).

[Biomass samples]

Pieces of ^{13}C-labeled cellulose sheet was incubated with methane fermentation sludge (50 ml, KAJIMA CORPORATION) at constant temperature of 55 ºC with stirring. At the timing of 0, 13, 24, 37, 42, 48, 54, 60, 66, 72, 84, 90, 96, 108, 114, 120 hours after incubation started, the sludge was corrected. The corrected sludge was centrifuged and separated into precipitate and supernatant. The precipitate was dried up in vacuum and used for solid state NMR measurements.

・Solid state NMR measurements

^{13}C CP/MAS and DARR was carried out on a 500 MHz standard bore spectrometer operating at room temperature (298K). The MAS spinning speed was set to 12000Hz.

・Statistical analysis

About 100 million base pairs of the DNA sequences targeted for 16S rRNA genes were determined by next generation sequencer (Illumina GA-II) in each degradation step, and the sequencial data was analysed by our original database, namely E-class. E-class can categorize based on the taxa of bacteria or family of cellulose binding module (CBM) from the very large sized sequence. The hit-number of each taxa or family and the data matrix of solid state NMR spectra were correlated using our original web tool HetMap. Solid state 2D DARR spectra were binned by our original web tool FT2DB (like Fig.1), and minus peaks and diagonal peaks were removed by Excel. The 2D data matrix was analysed by principal component analysis (PCA) using free software R. (E-class, HetMap and FT2DB are publically available via our web site ECOMICS https://database.riken.jp/ecomics/)

RESULTS AND DISCUSSION

^{13}C CP/MAS spectra in the each degradation step were measured at 298K, with spinning speed of 12000 Hz (Fig.2). Compared the spectra of 0 hour with that of 13 hours after the incubation started, the ratio of signal intensity was changed. Especially, in C6 carbon signal at 65 ppm and in C2, 3 or 5 carbon signals at around 72 ppm with short contact time, the changing tendency was remarkable. The effect of cross polarization depends mainly on the distance from ^{1}H, so the state around their carbons was thought to be changed.

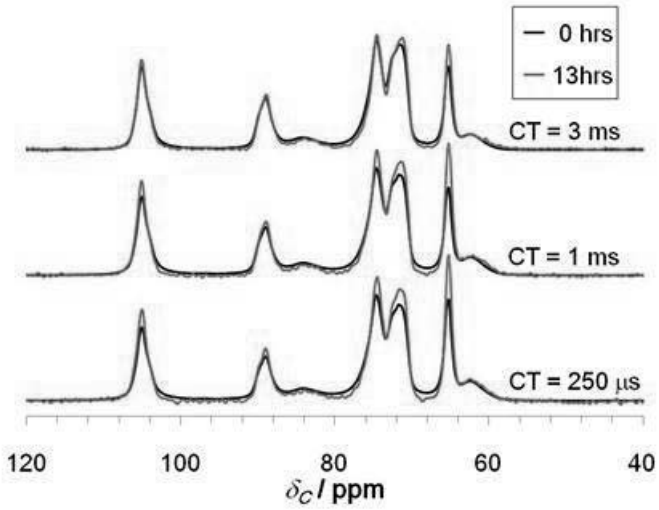

Fig. 2 Example of solid state NMR ^{13}C CP/MAS (MAS = 12000 Hz) spectra of cellulose in microbial ecosystem. Spectral intensity was normalized by all the area from 0 ppm to 200 ppm. Contact time of cross polarization was varied (250 μs, 1 ms, 3 ms).

For the search of candidate CBM or bacteria that is responsible for cellulose degradation, correlation analysis was performed with the hit number of CBM or bacteria class categorized by E-class and solid state ^{13}C CP/MAS spectra in all sampling steps (Fig. 3). CBM 3/6/22/25 were negatively correlated with cellulose degradation (decrease of ^{13}C CP/MAS signals), as well as positively correlated with bacterial class such as *Clostridia* and *Molicutes*.

In addition, along with the degradation of cellulose, signals of 10 – 60 ppm and 175 ppm in solid NMR spectra were increased. The signals of 10 – 50 ppm, 50－60 ppm and 175 ppm were thought to include protein side chain signals and lipid CH_2 signals, protein back bone signals, and protein C=O signal, respectively. It could be thought as that cellulose was incorporated into bacterial body and the increasing signals were derived from some or one of candidate bacteria..

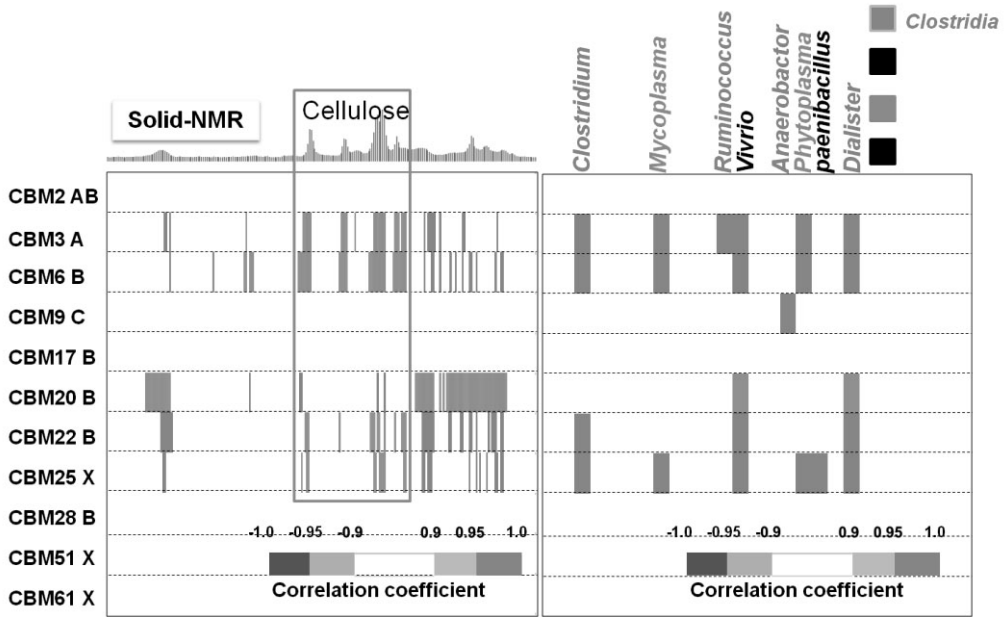

Fig. 3 Heat map of the correlation between CBM and Solid state NMR spectrum (left), and the correlation between CBM and bacterial class (right).

For getting more information not only on the amount of components, we focused on cellulose structure changing with degradation. As the first step for the analysis of the structural change of cellulose depending on degradation time, the method to extract the change of polymer cellulose C-C linkage and distance was investigated. DARR experiment can estimate the ^{13}C-^{13}C distance from the peak intensity or area and it is known as high quantitative experiment. Therefore, DARR experiment was adopted. But in general, 2D peaks of solid state NMR data were difficult to separate. For the analysis of cellulose-structural modulation, changing components are necessary to be separated. Then, we attempted to analyse 2D principal component analysis (PCA) of DARR spectra measured with modified cellulose and to visualize the change of structure in the 2D loading plot. In score plot, Iα structure was separated with PC1 and the differences of pre-treatment were exhibited in PC2 direction. In loading plot, PC1and PC2 components were consistent with the assignment of peaks.

We will discuss about the applicability of this method to the analysis of the cellulose degradation complex in microbial flora, and further analysis for the degradation product in each sampling time to combine the metabolic profiles with solution state NMR data will be presented.

References

1. Kikuchi, J. et al. “ECOMICS: ECosytem trans-OMICS tools and methods for complex environmental samples and datasets” ***J. Ecosys. Ecogr***. (in press).
2. Nakanishi, Y. Et al. “Dynamic omics approach identifies nutrition-mediated microbial interactions” ***J. Proteome Res***. 10, 824-831 (2011).
3. Sekiyama, Y. et al. “Profiling polar and semi-polar plant metabolites throughout extraction processes using a combined solution-state and HR-MAS NMR approach” ***Anal. Chem***. 82, 1643-1652 (2010).

cellulose, Solid-state NMR, microflora

P-085 Simulation of Magic-Angle Spinning Solid-State NMR Spectral Fitting for Proteins and Peptides using Replica-Exchange Monte Carlo Algorithm

Keisuke Ikeda[1], Tomoshi Kameda[2], Ayako Egawa[1], Hideo Akutsu[1], and Toshimichi Fujiwara[1]

[1]Institute for Protein Research, Osaka University and
[2]Computational Biology Research Center, AIST.

ABSTRACT: We report a simulation procedure for analyzing magic-angle spinning solid-state NMR spectra for structural analysis of proteins and peptides. Experimental 2D ^{13}C-^{13}C spectra were fitted by calculated spectra. We employed Markov-chain Monte Carlo algorithm combined with an advanced sampling replica-exchange technique for exploring a chemical shift space in order to minimize a difference between simulated and observed spectra. Signal intensities of spectral peaks were calculated by the average Hamiltonian theory and rate matrix analysis of magnetization transfer. The simulation determined the $^{13}C^{\alpha}$, $^{13}C^{\beta}$, and $^{13}C'$ chemical shifts for the proteins with precisions in the order of line widths of the peaks. We also obtained the information of secondary structures from the estimated ^{13}C chemical shifts. The simulations were robust to spectral noises and calculation errors. Our methodology can be utilized for analyzing structures of non-crystalline proteins from unresolved MAS SSNMR spectra in which peaks are heavily overlapped. In addition, the method does not require peak-picking, prerequisite for manual assignments.

INTRODUCTION

Signal assignment is required for analyzing structures and dynamics of proteins and peptides by magic-angle spinning solid-state NMR. Owing to recent developments in multidimensional experiments and sample preparations such as selective isotope labeling, we can assign signals from spectra of highly homogeneous samples such as crystalline proteins with line widths of <0.5 ppm. However, overlaps of signals in the spectra due to larger line widths of >1 ppm in non-crystalline proteins still make it difficult to perform signal assignments and subsequent structural analysis.

Here, we developed a spectral fitting simulation for automated signal assignments of C^{α}, C^{β}, and C' chemical shifts and analysis of protein structures from unresolved MAS SSNMR spectra. ^{13}C-^{13}C spectra were calculated to fit observed spectra. The replica-exchange technique was employed for effectively sampling a chemical shift space and assigning signals. We applied our simulation to various sizes of proteins and showed that the simulation successfully estimated the chemical shifts of the proteins. Secondary structures of the proteins were determined using the assignments. We also evaluated effects of spectral information, line widths, spectral noises, and calculation errors on the accuracy of the estimated chemical shifts.

METHODS

Algorithm. The inputs for the simulation were a sequence of amino acids for a protein of interest,

signal assignment, spectral simulation, signal overlap

2D ^{13}C-^{13}C spectral data, and experimental parameters such as mixing times for magnetization transfer. The outputs were estimated chemical shifts for the protein, calculated spectra, and pseudo-energies. A state, an assumed chemical shift assignment for the protein, was sampled by the Monte Carlo simulation. The energy of the state was defined as a residual sum of squares between the observed spectra of input and those simulated from the chemical shifts. The signal intensities of cross peaks were calculated using the average Hamiltonian theory and rate matrix analysis of magnetization transfer. In the replica-exchange algorithm, *N* parallel MC simulations were independently performed at various temperatures. These temperatures were attempted to be exchanged between the MC simulations at intervals of every 100,000 MC steps. We repeated the replica-exchange of 2000-4000 cycles to converge the system. Finally, we obtained the average chemical shifts of the most populated, low-energy states at the lowest temperature by principal component analysis of the states.

Test simulations. Six proteins whose chemical shift assignments were deposited in the Biological Magnetic Resonance Data Bank (BMRB) database were used for the test simulations validating our methods. The sizes of the proteins were ranging from 38 to 87 amino acid residues. The ^{13}C-^{13}C spectra of these proteins were calculated from the assigned chemical shifts with assumed line widths and then the fitting simulations were performed.

RESULTS AND DISCUSSION

We conducted spectral fitting simulations for 2D ^{13}C-^{13}C spectra of intra- and inter-residue C^{α}_{i}-C'_{i}, C^{α}_{i}-C^{β}_{i}, C^{α}_{i+1}-C^{α}_{i}, C^{α}_{i+1}-C'_{i}, C^{α}_{i+1}-C^{β}_{i}, and C^{β}_{i+1}-C'_{i} correlation experiments. The spectra with a line width of 1.5 ppm exhibited significant overlaps of cross peaks. The estimated chemical shifts for the 6 proteins by the test simulations showed root-mean-square differences (RMSDs) of 0.5-1.5 ppm from those in the BMRB database. The RMSDs were increased with increasing the size of the proteins, indicating that the size of the sampling space and the overlaps in the spectra were affecting the accuracy of the estimated chemical shifts. However, the increase in line widths of the spectra up to 2.2 ppm did not significantly affect the RMSDs.

For quantifying the contributions of the spectral information to the accuracy of estimated chemical shifts, we performed the test simulations by removing a spectrum from the 6 ^{13}C-^{13}C correlation spectra. The chemical shift RMSDs were increased without the intra- and inter-residue C^{α}-C^{β} correlation spectra, suggesting that these correlations had critical information for determining the chemical shifts.

In real situations, observed spectra contain noises and the calculation of signal intensities includes errors. The RMSDs from the test simulations with the spectral noises and calculation errors of 5% were almost the same with those obtained by the simulation without noises and errors. The results revealed the simulations to be robust to the noises and the errors.

The protein secondary structures could be predicted from the estimated ^{13}C chemical shifts. The regions of α-helix and β-sheet structures were determined with an accuracy of >70% by plotting secondary shifts of the assignments.

In conclusion, we developed the robust simulation of the automated signal assignments and the structural analysis from MAS SSNMR spectra in which peaks were overlapped. The present strategy is applicable for the MAS SSNMR spectra of non-crystalline proteins such as amyloid fibrils and membrane proteins with larger line widths than those of crystalline samples.

P-086 NMR-based conformational analysis of sphingomyelin in lipid rafts

Toshiyuki Yamaguchi, Yoshiko Maeta, Nobuaki Matsumori and Michio Murata
Department of Chemistry, Osaka University

ABSTRACT

Lipid rafts[1] (Figure 1) are a membrane microdomain typically enriched in sphingomyelin (SM) and cholesterol (Chol). They are assumed to be implicated in a number of cellular processes such as signal transduction, protein sorting and cholesterol shuttling. In spite of such biological significances, the way in which raft lipids self-assemble to form a nanometer-scale organization is still far from understood largely due to the rapid association and dissociation equilibrium of lipid molecules in rafts. To gain a fundamental understanding of the molecular interactions in lipid rafts, exploration of structures and dynamics of SM in membrane environments is crucial.

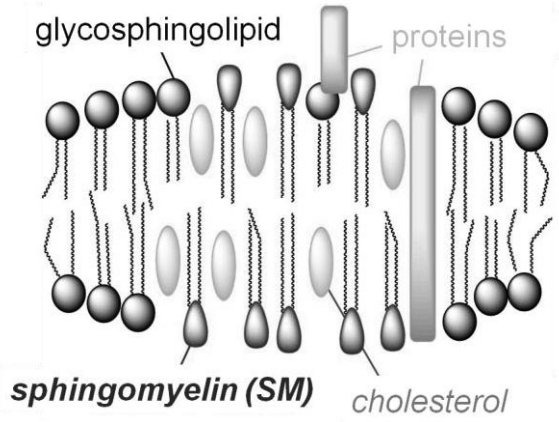

Figure 1 schematic model of lipid rafts

In this study, to deduce the structure basis of raft formation, particularly the conformation of SM, we carried out REDOR[2] (Rotational Echo DOuble Resonance) experiments, which are a solid-state NMR method to measure the distance between two selected heteronuclei based on the dipolar coupling. Some ^{15}N- and/or ^{13}C labeled SMs were synthesized for REDOR (Figure 2). First, to determine the orientation of the amide plane of SM with the respect to the membrane normal, we measured the dipolar couplings between ^{15}N and ^{13}C nuclei using ^{15}N-labelled SMs (**1-3**) by ^{13}C{^{15}N}REDOR experiments. The results indicate that the amide plane of SM hardly undergoes orientational change with respect to the membrane normal in the presence or absence of Chol, whereas the order of amide part is higher with Chol than that without Chol.

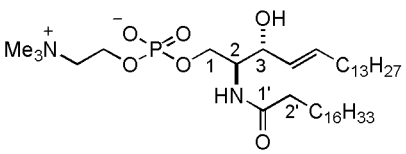

2-^{15}N-SM (**1**) 1'-^{13}C-SM (**4**)
1'-^{13}C-2-^{15}N-SM (**2**) 2'-^{13}C-SM (**5**)
2'-^{13}C-2-^{15}N-SM (**3**) 3-^{13}C-SM (**6**)

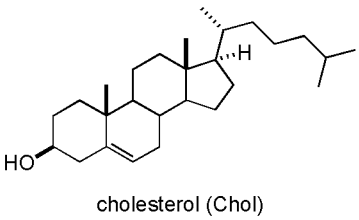

Figure 2 structures of sphingomyelin (SM) and cholesterol (Chol)

Then, ^{31}P{^{13}C}REDOR experiments using ^{13}C-labeled SMs (**4-6**) were carried out to elucidate the conformation around the phosphate group of SM (Figure 3). In the case of C1'-labelled SM (**4**), the magnitude of REDOR dephasing was higher without Chol (Figure 3A) than that with Chol (Figure 3B), whereas, when using C3-labeled SM (**6**), the magnitude was lower without Chol

(Figure 3C) than with Chol (Figure 3D) These results may imply that SM changes the orientation of the phosphate group by forming a complex with Chol; the phosphate group tends to face to C1' without Chol and come close to C3 with Chol. Then, the orientation of the phosphate group of SM was analyzed based on the magnitude of dipolar coupling obtained by fitting experimental data to the theoretical REDOR curve. As a result, the conformations of SM in membrane with and without Chol were successfully deduced; a conformer with higher order is more populated in Chol-containing raft-like phase, whereas another conformer with lower order being dominant in Chol-free non-raft phase. A more detailed NMR analysis is under way to further elucidate the conformation of SM in membrane.

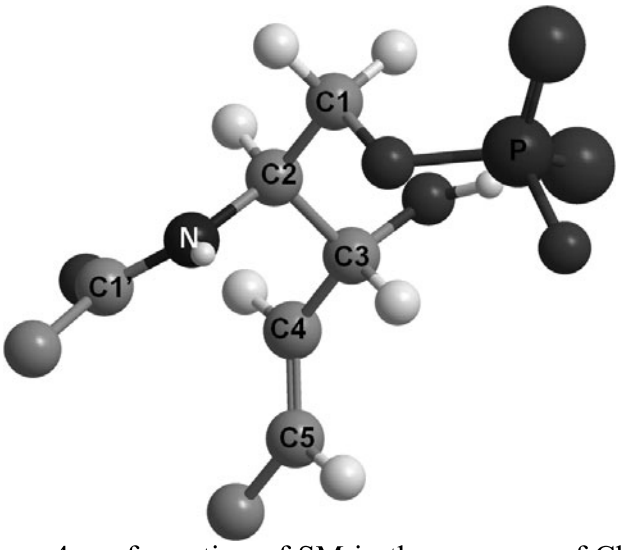

Figure 4 conformation of SM in the presence of Chol in membrane deduced from REDOR experiments

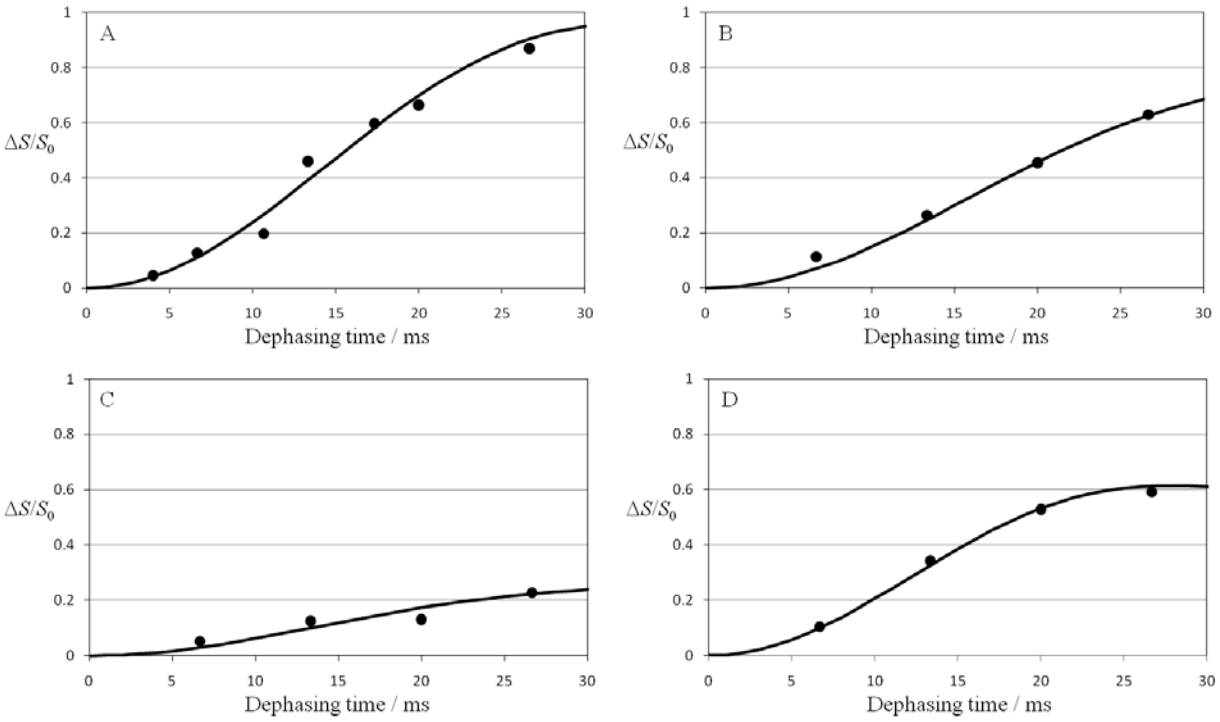

Figure 3 $^{31}P\{^{13}C\}$REDOR plot (●) experimental data (—) theoretical curve
(A) 1'-^{13}C-SM, (B)1'-^{13}C-SM/Chol (1/1), (C) 3-^{13}C-SM, (D) 3-^{13}C-SM/Chol (1/1)

References
1) Simons, K.; Vaz, W. L. C. *Annu. Rev. Biophys. Biomol. Struct.* **2004**, *33*, 269-295.
2) Gullion, T.; Schaefer, J. *Adv. Magn. Reson.* **1989**, *13*, 57-83.

Sphingomyelin, Lipid rafts, Conformational analysis

P-087 Solid-state NMR analysis of the molecular interaction of Pradimicin A with Ca^{2+} ion and mannose

Takashi Doi[1], Yuichi Masuda[1], Keita Yamada[1], Yu Nakagawa[2], Yukishige Ito[2, 3], Yasuhiro Igarashi[4] and K. Takegoshi[1]

[1]Graduate School of Science, Kyoto University
[2]Synthetic Cellular Chemistry Laboratory, RIKEN Advanced Science Institute
[3]Japan Science and Technology Agency, ERATO, Ito Glycotrilogy Project
[4]Biotechnology Research Center, Toyama Prefectural University

Pradimicin A (PRM-A) is a natural antibiotic, which specifically binds D-mannopyranoside (Man) in the presence of Ca^{2+} ion to form the aggregate of the ternary complex. We analyzed the aggregate by solid-state NMR to examine the molecular interaction of PRM-A with Ca^{2+} ion and Man. A combination of ^{113}Cd-NMR using $^{113}Cd^{2+}$ ion as a surrogate for Ca^{2+} ion and 2D ^{13}C dipolar-assisted rotational resonance (DARR) using biosynthetically ^{13}C-enriched PRM-A revealed that PRM-A binds Man in a Ca^{2+}-mediated manner through its carboxylate group. The present study is a rare example of solid-state NMR analysis of site specific molecule interaction between small molecules (PRM-A and Man).

1. Introduction

Pradimicin A (PRM-A, Fig. 1), a natural non-peptidic antibiotic isolated from actinomycetes,[1] shows lectin-like properties of recognizing D-mannopyranoside (Man) in the presence of Ca^{2+} ion.[2] Recently, PRM-A has been attracted as a conceptually novel drug candidate for human immunodeficiency virus (HIV).[3] Although the anti-HIV effects are explained by its specific binding to Man residues of glycans on the viral envelope, the mechanism of Man recognition by PRM-A remains unclear due to the aggregate-forming propensity of PRM-A. In this study, we analyzed the solid aggregate consisted of the PRM-A/Ca^{2+}/Man complex by solid-state NMR to examine the molecular interaction of PRM-A with Ca^{2+} ion and Man.

2. Analysis of the role of Ca^{2+} ion using solid-state ^{113}Cd NMR spectroscopy

Previous works indicated that Ca^{2+} ion binds two molecules of PRM-A, and the carboxy group of PRM-A was proposed as the putative binding site for the Ca^{2+} ion.[4] However, it still remains unclear whether the role of the Ca^{2+} ion is solely to bridge two PRM-A molecules, or whether it also participates in Man binding. In order to investigate this issue, we carried out a solid-state ^{113}Cd NMR spectroscopic investigation with $^{113}Cd^{2+}$ ion with a spin of 1/2 as a surrogate probe for Ca^{2+} ion with a spin of 7/2. As $^{113}Cd^{2+}$ and Ca^{2+} ions have the same formal charge and similar ionic radii, and NMR measurement and analysis of ^{113}Cd nuclei are much easier than those of Ca, ^{113}Cd NMR spectroscopy has proven to be an excellent technique for the examination of the Ca^{2+} environments present in biological systems.

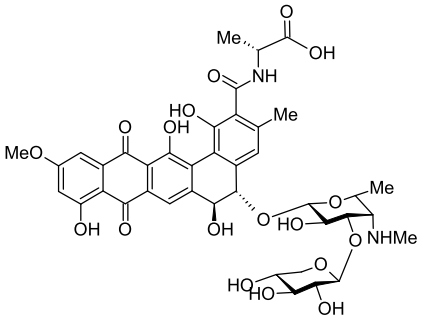

Fig. 1 Pradimicin A (PRM-A)

Key Words: Molecular interaction, Pradimicin A, Solid-state NMR

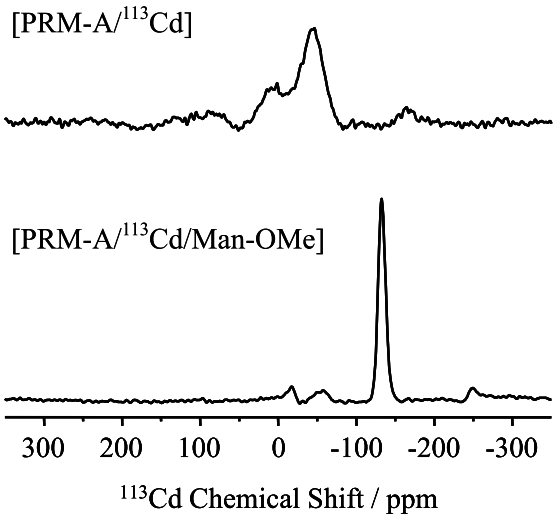

Fig. 2 Solid-state CP/MAS ^{113}Cd NMR spectra of PRM-A/^{113}Cd aggregates

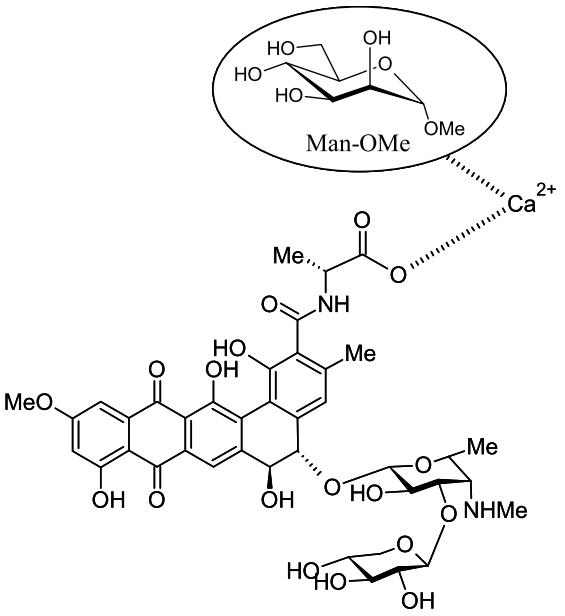

Fig. 3 Ca^{2+}-mediated binding model of PRM-A with Man

We prepared the solid aggregates of binary [PRM-A/$^{113}Cd^{2+}$] and ternary [PRM-A/$^{113}Cd^{2+}$/Man-OMe] complexes, and conducted CP/MAS ^{113}Cd NMR spectroscopic experiments with them. Whereas the binary [PRM-A/$^{113}Cd^{2+}$] complex exhibited a broad ^{113}Cd signal around δ = -50 ppm, the ternary [PRM-A/$^{113}Cd^{2+}$/Man-OMe] complex exhibited a sharp ^{113}Cd signal at δ = -135 ppm (Fig. 2). The large difference in chemical shift of ^{113}Cd signals between the binary and the ternary complexes indicates that $^{113}Cd^{2+}$ coordination has changed upon Man-OMe binding. Since ^{113}Cd signals upfield of δ = -100 ppm are observed only for $^{113}Cd^{2+}$ coordinated with more than six oxygen ligands,[5] it is reasonable to assume that Man-OMe coordinates as an additional ligand to the $^{113}Cd^{2+}$ ion in the binary [PRM-A/$^{113}Cd^{2+}$] complex. From these results, we proposed the Ca^{2+}-mediated binding model of PRM-A with Man-OMe, in which Man-OMe is located in the proximity of the Ca^{2+}-bound carboxy group of PRM-A (Fig. 3).

3. Detection of close interactions of PRM-A with Man-OMe by two-dimensional ^{13}C dipolar assisted rotational resonance (2D ^{13}C DARR)

To obtain more concrete experimental support for our model, we performed two-dimensional ^{13}C dipolar assisted rotational resonance (2D ^{13}C DARR)[6] experiments to examine proximities between Man-OMe and the D-alanine moiety of PRM-A, which contains the Ca^{2+}-bound carboxy group. The DARR method has been shown to detect weak ^{13}C-^{13}C coupling in the presence of strong coupling due to directly bound carbon atoms, and dipolar interactions between ^{13}C nuclei that are located within 6 Å of one another can be detected as cross-peaks in the 2D DARR spectrum.

Using biosynthetically ^{13}C-enriched PRM-As ($^{13}C_3$-PRM-A and $^{13}C_2$-PRM-A, Fig. 4)[7] and $^{13}C_6$-Man-OMe, we prepared the solid aggregates of their [PRM-A/$^{113}Cd^{2+}$/Man-OMe] complexes. 2D DARR spectra of ternary [$^{13}C_3$-PRM-A/$^{113}Cd^{2+}$/$^{13}C_6$-Man-OMe] complex showed intermolecular cross-peaks between the carbon signals for the D-alanine moiety of PRM-A and

those for Man-OMe (Fig. 5a). This result strongly indicates that the D-alanine moiety of PRM-A is close to Man, supporting our binding model. On the other hand, 2D DARR spectra of ternary [$^{13}C_2$-PRM-A/$^{113}Cd^{2+}$/$^{13}C_6$-Man-OMe] complex showed only intramolecular cross-peaks (Fig. 5b). This result negates nonspecific binding of PRM-A with Man-OMe because the cross-peaks between carbon signals for the D-alanine moiety of PRM-A and those for Man-OMe truly arise from specific interactions among them.

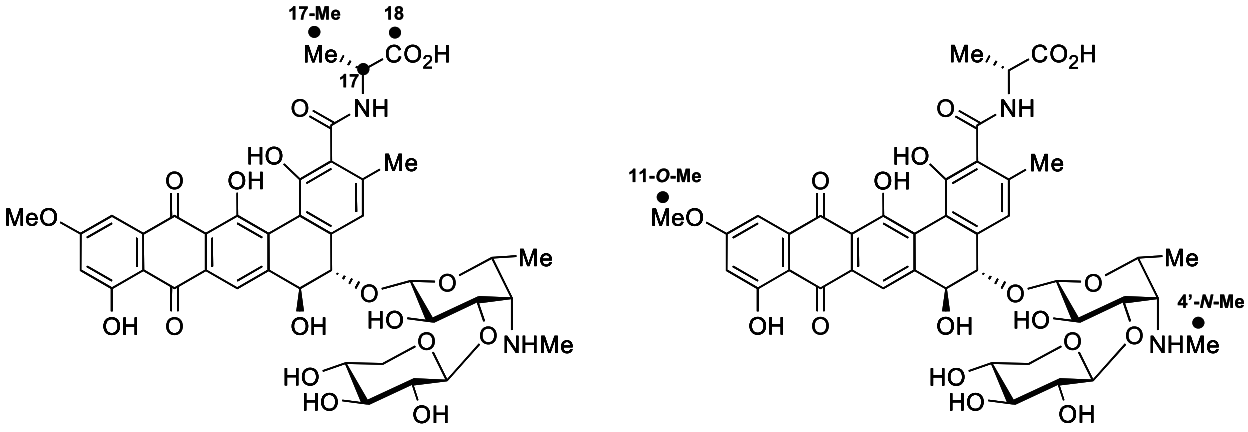

(a) $^{13}C_3$-PRM-A (b) $^{13}C_2$-PRM-A

Fig. 4 ^{13}C-enriched PRM-As

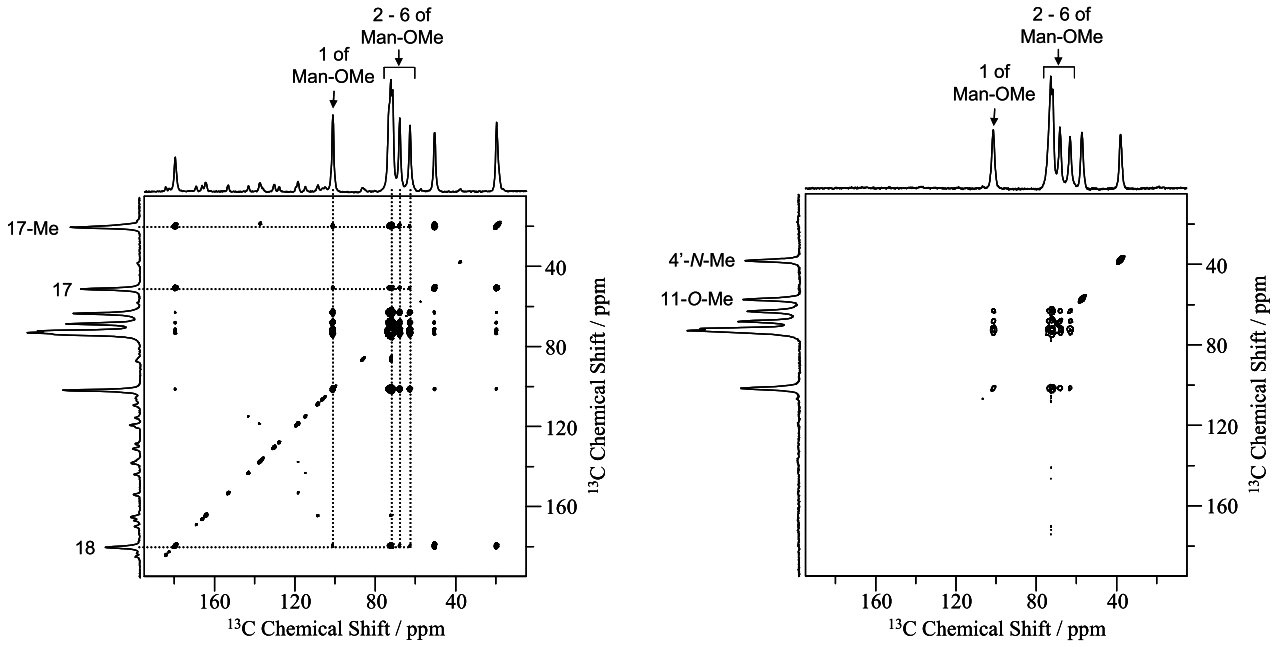

(a) [$^{13}C_3$-PRM-A/Ca^{2+}/$^{13}C_6$-Man-OMe] (b) [$^{13}C_2$-PRM-A/Ca^{2+}/$^{13}C_6$-Man-OMe]

Fig. 5 2D DARR spectra of the ternary complexes of ^{13}C-enriched PRM-As with Ca^{2+} and $^{13}C_6$-Man-OMe at the mixing time of 500ms. Black circles indicate ^{13}C-enriched sites.

4. Conclusion

In this work, we investigated the Ca^{2+}-dependent Man binding of PRM-A in the solid-state. On the basis of solid-state ^{113}Cd NMR and 2D DARR analysis, we propose an unprecedented Ca^{2+}-mediated binding model of PRM-A with Man (Fig.3). This results is the first solid evidence that the D-alanine moiety of PRM-A is the Man-binding region.[8] The present study provides a clue toward the full elucidation of the molecular basis of Man recognition by PRM-A. In order to clarify more precise binding mode of PRM-A with Man, further investigations are currently in progress.

5. References

[1] T. Oki, M. Konishi, K. Tomatsu, K. Tomita, K. Saitoh, M. Tsunakawa, M. Nishio, T. Miyaki, H. Kawaguchi, *J. Antibiot*. **1988**, *41*, 1701-1704.

[2] a) Y. Sawada, K. Numata, T. Murakami, H. Tanimachi, S. Yamamoto, T. Oki, *J. Antibiot*. **1990**, *43*, 715-721; b) Y. Fukagawa, T. Ueki, K. Numata, T. Oki, *Actinomycetol*. **1993**, *7*, 1-22.

[3] J. Balzalini, *Nat. Rev. Microbiol*. **2007**, *5*, 583-597.

[4] a) T. Ueki, K. Numata, Y. Sawada, T. Nakajima, Y. Fukagawa, T. Oki, *J. Antibiot*. **1993**, *4*6, 149-161; b) T. Ueki, K. Numata, Y. Sawada, M. Nishio, H. Ohkura, H. Kamachi, Y. Fukagawa, T. Oki, *J. Antibiot*. **1993**, *4*6, 455-464.

[5] a) M. F. Summers, *Coord. Chem. Rev*. **1988**, *86*, 43-13; b) K. McAteer, A. S. Lipton, P. D. Ellis, in *Encyclopedia of Nuclear Magnetic Resonance*, (Eds.: D. M. Grant, R. K. Harris), John Wiley & Sons, Chichester, **1996**, pp. 1085-1091.

[6] a) K. Takegoshi, S. Nakamura, T. Terao, *Chem. Phys. Lett.* **2001**, *344*, 631-637; b) K. Takegoshi, S. Nakamura, T. Tamao, *J. Chem. Phys*. **2003**, *118*, 2325-2341.

[7] M. Kakushima, Y. Sawada, M. Nishio, T. Tsuno, T. Oki, *J. Org. Chem.* **1989**, *54*, 2536-2539.

[8] Y. Nakagawa, Y. Masuda, K. Yamada, T. Doi, K. Takegoshi, Y. Igarashi, Y. Ito, *Angew. Chem. Int. Ed*. **2011**, *50*, 6084-6088.

P-088 Solid-state NMR structural analysis of transmembrane halobacterial transducer *p*HtrII

Ayako Egawa[1], Keisuke Ikeda[1], Momoko Yoneyama[1], Kokoro Hayashi[2], Chojiro Kojima[1], Hideo Akutsu[1] and Toshimichi Fujiwara[1]
[1]Institute for Protein Research, Osaka University
[2]Graduate School of Biological Sciences, Nara Institute for Science and Technology

ABSTRACT

Transmembrane protein *p*HtrII from *N. pharaonis* is a transducer which binds to phoborhodopsin. We studied uniformly ^{13}C, ^{15}N labeled 159-residues *p*HtrII by high-resolution solid-state NMR. We have assigned ^{13}C signals of immobile regions by using spin diffusion at –10°C. Signal assignments of mobile protein segments were performed by *J*-coupling-based CC TOCSY experiments for the NOE enhanced initial ^{13}C polarization. These CA chemical shifts indicate 80% and 30% α-helix formation in transmembrane and extramembrane, respectively. The inter-residue and intermolecular information will be confirmed by amino-acid selectively labeled *p*HtrII.

INTRODUCTION

Pharaonis phoborhodopsin (*p*pR) is a photoreceptor of *N. pharaonis* bacteria. A transducer protein *p*HtrII forms a complex with *p*pR in cell membranes. The light excitation of phoborhodopsin is transmitted to the cytoplasm through *p*HtrII to promote negative phototaxis. It was considered that the structure change of the connected HAMP domain in *p*HtrII provides an important role for signal transduction. However, the mechanism still remains to be clarified.

Crystal structure of the transmembrane region of *p*HtrII (24-82 residues) as complex with *p*pR has been reported [1]. The extramembrane region of *p*HtrII cannot be crystallized because of the dynamic structure. Therefore solid-state NMR is a powerful method for the structural analysis of mobile regions. Here we have performed the structure analysis of uniformly ^{13}C, ^{15}N labeled *p*HtrII (1-159) in deuterated DMPC bilayers by solid-state NMR.

MATERIAL AND METHODS

Uniformly ^{13}C, ^{15}N labeled *p*HtrII (1-159) were overexpressed in *E. coli* BL21 (DE3) cells using M9 minimal medium. The obtained *p*HtrII was purified by Ni^{2+}-NTA agarose column and gel filtration. Purified *p*HtrII was reconstituted into DMPC bilayers [2]. The precipitate was packed in a 3.2-mm rotor by ultracentrifugation for solid-state NMR experiments.

Solid-state NMR spectra were recorded on a Varian Infinity-plus 600 and 700 spectrometers equipped with a MAS probe. 2D ^{13}C spin-diffusion spectra and *J*-coupling-based CC NOE-TOCSY spectra were recorded under MAS at –10°C and 10°C, respectively. 2D $(C^{\alpha}C^{\beta})_{i+1}$-$(C'C^{\alpha})_i$ experiments for inter-residue assignments were performed at –60°C.

Membrane protein

RESULTS AND DISCUSSION

At first, we have assigned ^{13}C signals of the immobile regions in *p*HtrII (1-159) by using ^{13}C-^{13}C spin diffusion under DARR at −10°C. Signal assignments of mobile protein segments making up about 70% of *p*HtrII (1-159) were performed by *J*-coupling-based CC TOCSY experiments for the CH NOE enhanced ^{13}C polarization at 10°C. Additionally we performed *J*-coupling-based HC-INEPT and HCC-TOCSY experiments in order to assign ^{1}H signals of mobile protein segments. The signal assignment can be confirmed by using amino-acid selectively labeled *p*HtrII. The Cα and CO chemical shifts of assigned resonances indicated that *p*HtrII (1-159) mainly formed 80% and 30% α-helix structure in transmembrane and extramembrane, respectively.

We carried out HCC-TOCSY experiments for *p*HtrII in the membrane fraction before the solubilization with detergent. Spectral lines were very sharp with linewidths about 50 Hz, indicating that *p*HtrII molecules are more homogeneous and mobile in the membrane fraction than in the reconstituted DMPC membrane. This molecular state also allowed the acquisition of HNCOCA inter-residue correlations. In the membrane fraction the major secondary structure was α-helix with a definite minor one existed. For simplicity in the assignments, U-[^{13}C, ^{15}N \ F,L,Y,K,V] *p*HtrII membrane fraction was used.

Distance constraints were obtained from spin-diffusion experiments based on dipolar couplings. For this purpose, we were carrying out water-edited spin-diffusion experiments for detecting water accessible regions of *p*HtrII.

Inter-residue assignments were performed from 2D $(C^{\alpha}C^{\beta})_{i+1}$-$(C'C^{\alpha})_{i}$ experiments. Additionally we obtained partially inter-residue correlations from spin-diffusion experiments at 400 ms [Fig.1]. Finally, 1D NHHC experiments were conducted for intermolecular information. The results indicated the signals derived from inter-dimer correlations.

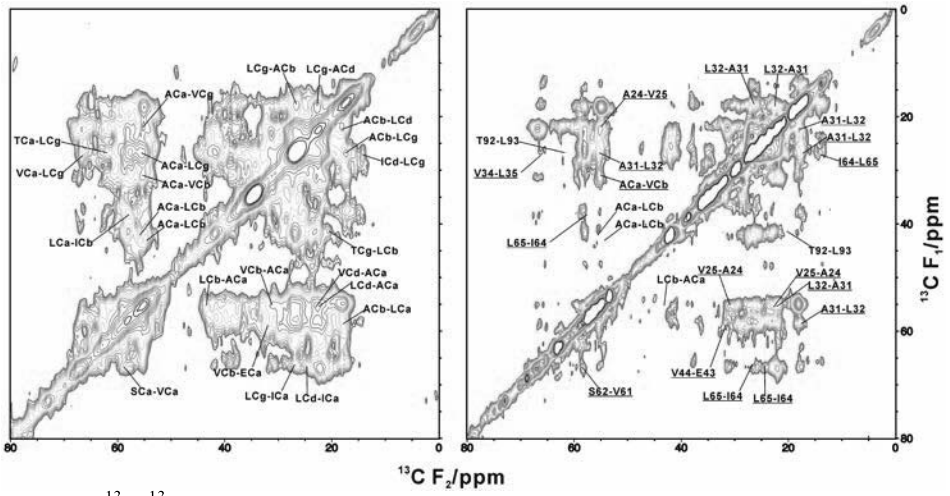

Fig1. 2D ^{13}C-^{13}C dipolar correlation spectra at 400 ms. Experiments were carried out at −60°C (left) and −10°C (right) in probe temperature.

REFERENCES

1. Gordeliy, V.I. *et al.* (2002) *Nature*, **419**:484-487.
2. Hayashi, K. *et al.* (2007) *Biochemistry*, **46**:14380-14390.

P-089 Y Intermolecular Structure Analysis in Alanine Oligomers by ^{13}C, ^{15}N, and ^{17}O Gauge-Including Projector Augmented-Wave (GIPAW) Calculations

Furitsu Suzuki [1], Akihiro Aoki [2], Tetsuo Asakura [2], Yusuke Nishiyama [3] and Hironori Kaji[1]

[1]Institute for Chemical Research, Kyoto Univ., [2]Department of Biotechnology, Tokyo Univ. of Agriculture and Technology, and [3]JEOL RESONANCE Inc.

ABSTRACT:

The structural analysis was carried out for the crystals of alanine tripeptides in the anti-parallel (AP-Ala_3) and parallel (P-Ala_3) β-sheet forms through the combined use of solid-state NMR spectroscopy and gauge-including projector augmented-wave (GIPAW) calculations. Different from the chemical shift calculations by conventional gauge-including atomic orbital (GIAO) method for a single molecule, the GIPAW method can be carried out for the crystal structure under the periodic boundary conditions (PBC) and therefore, the intermolecular interaction can be included in the chemical shift calculations. The chemical shifts calculated by GIPAW method are found to be well reproduced the experimental results. From the study, we show that the combined use of these methods can be a powerful method for the intra- and inter-molecular analysis of materials, including alanine oligomers.

Introduction

β-sheet structure is one of the typical structures found in many biological macromolecular structures. In relation to the function of the biological macromolecules, it is important to clarify whether intermolecular packing is parallel or anti-parallel. Recently, analysis of the fibrous structures of amyloidal peptide is very active and it has been reported that the formation of parallel and anti-parallel β-sheet structures depends on the kinds and lengths of the amino acids, but the systematic relationship have not been well understood. The fibrous structures are less likely to form single crystal and therefore solid-state NMR, which provides structural information even for disordered materials, is effective way to analyze the structures in detail.

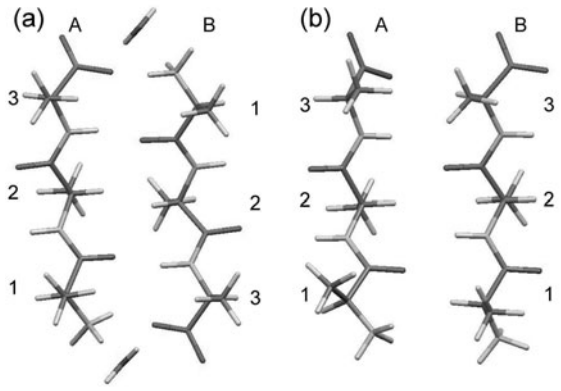

Fig. 1. The atomic level structures of alanine tripeptide with (a) anti-parallel (AP-Ala_3) and (b) parallel (P-Ala_3) β-sheet forms. Alphabet A or B shows the distinction of chains, and number 1-3 shows the three types of residues.

In this study, we demonstrate the structural investigation for the crystals of alanine trimers in the parallel (P-Ala_3) and anti-parallel (AP-Ala_3) forms (Fig. 1) as a model of biological amyloidal

GIPAW, Chemical shift calculation, Alanine oligomer

peptides through the combined use of solid-state ^{13}C, ^{15}N, ^{17}O NMR spectroscopies [1-3] and the GIPAW calculations recently developed by Pickard and Mauri [4]. The GIPAW calculations allow to calculate NMR parameters in periodic boundary condition within the pseudopotential approximation. From our previous researches, we have shown that the structural refinement of organic crystal structures obtained by the X-ray diffraction method is accomplishable by combined use of the solid state NMR spectroscopy and the GIPAW calculations [5].

Experimental section

Two kinds of geometry optimization procedure were applied for both the AP-Ala_3 and P-Ala_3 crystals under the periodic boundary condition. One is the optimization of the atomic coordinates only for protons, and another is the optimization of the atomic coordinates for all atoms. The generalized gradient approximation (GGA) for the exchange correlation energy using the Perdew, Burke and Ernzerhof (PBE) functional and ultrasoft pseudopotentials were used for geometry optimization and GIPAW calculations. All these calculations were carried out by the CASTEP program.

For comparison, isotropic chemical shifts calculations by GIAO method were carried out for single molecules, which were extracted from the X-ray diffraction and two kinds of optimized crystal structures as described above. GIAO calculations were performed by DFT method using the B3LYP/6-31G(d) level by Gaussian 09 program.

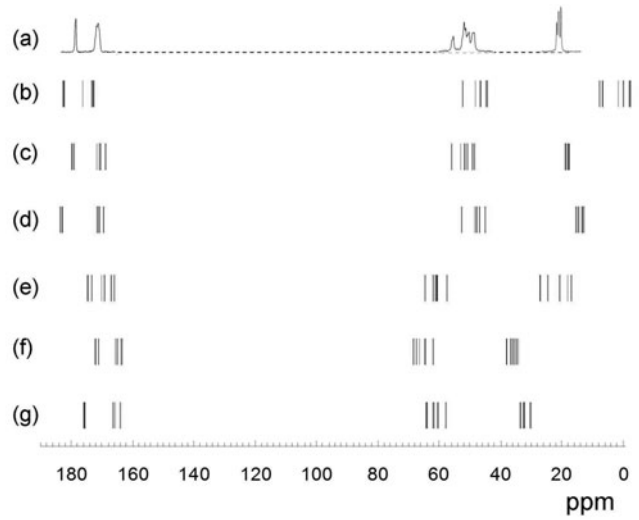

Fig. 2. (a) Experimental ^{13}C CP/MAS NMR spectrum of AP-Ala_3. Calculated isotropic chemical shifts of AP-Ala_3 by (b)–(d) GIPAW and (e)-(g) GIAO methods. Calculations were carried out for the crystal structure (b) by X-ray diffraction analysis without structural optimization, (c) after the optimization of the atomic coordinates only for protons, (d) after the optimization of the atomic coordinates for all atoms. The calculations of (e), (f), and (g) were carried out for single molecules extracted from the crystal structures used for the calculations of (b), (c), and (d).

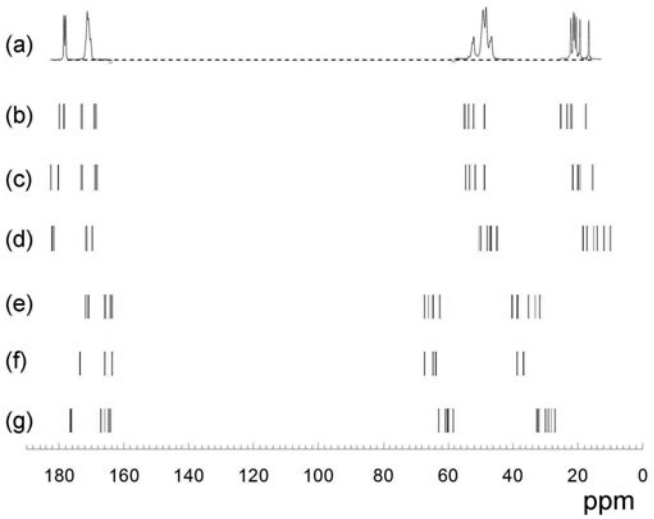

Fig. 3. (a) Experimental ^{13}C CP/MAS NMR spectrum of P-Ala_3. Calculated isotropic chemical shifts of P-Ala_3 by (b)–(d) GIPAW and (e)-(g) GIAO methods. Calculations were carried out for the crystal structure (b) by X-ray diffraction analysis without structural optimization, (c) after the optimization of the atomic coordinates only for protons, (d) after the optimization of the atomic coordinates for all atoms. The calculations of (e), (f), and (g) were carried out for single molecules extracted from the crystal structures used for the calculations of (b), (c), and (d).

Results and discussion

Fig. 2 shows the CP/MAS ^{13}C NMR spectra for AP-Ala_3 crystals [1]. Fig. 2 (b)-(d) and (e)-(g) shows the calculated isotropic chemical shifts by GIPAW method and GIAO method, respectively. Fig.3 also shows the experimental CP/MAS ^{13}C NMR spectra and calculated chemical shifts for P-Ala_3 crystals. It is found that calculated isotropic chemical shifts by GIAO method ((e)-(g) in Figs. 2 and 3) are not in good agreement with the experimental chemical shifts; calculated chemical shift ranges are narrower than the experimental chemical shift range.

On the other hand, the calculated isotropic chemical shifts by GIPAW method ((b)-(d) in Figs. 2 and 3) are in better agreement with the experimental chemical shifts. The best agreement is obtained for the crystal structure after the optimization of the atomic coordinates only for protons. These differences are considered as follows. Structures used in Figs. 2 (b) and 3 (b) are obtained by X-ray diffraction analysis, the position of hydrogen atoms unreliable. In comparison, structures used in Figs. 2 (c) and 3(c) are reliable because the coordinates of heavy atoms are obtained by the X-ray diffraction analysis and the atomic coordinates for protons are optimized by geometry optimization calculations. On the other hand, structures used in Figs. 2 (d) and 3 (d) are considered unreliable because the larger error in the coordinates by excessive structural optimization of the atomic coordinates for all atoms.

In addition, the merging and splitting of resonance lines in the region of methyl carbons including methyl carbon of 1-B residue appears in the most high-field side in Fig. 3 (a) and Fig. 3 (c) are well

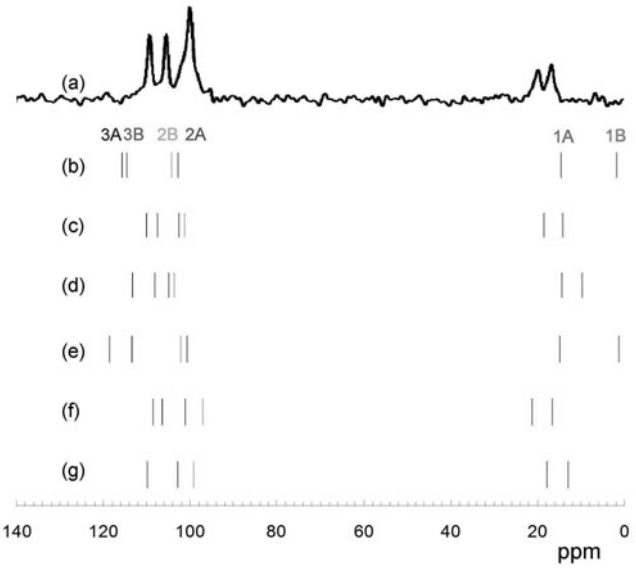

Fig. 4. (a) Experimental ^{15}N CP/MAS NMR spectrum of AP-Ala_3. (b)-(g) Calculated isotropic chemical shifts of AP-Ala_3 by GIPAW and GIAO methods. Calculations were carried out for the crystal structure (b) by X-ray diffraction analysis without structural optimization, (c) after the optimization of the atomic coordinates only for protons, (d) after the optimization of the atomic coordinates for all atoms. The calculations of (e), (f), and (g) were carried out for single molecules extracted from the crystal structures used for the calculations of (b), (c), and (d).

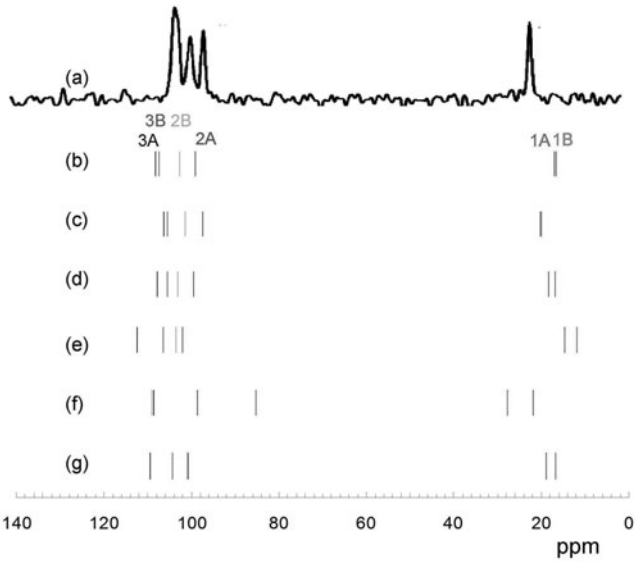

Fig. 5. (a) Experimental ^{15}N CP/MAS NMR spectrum of P-Ala_3. (b)-(g) Calculated isotropic chemical shifts of P-Ala_3 by GIPAW and GIAO methods. Calculations were carried out for the crystal structure (b) by X-ray diffraction analysis without structural optimization, (c) after the optimization of the atomic coordinates only for protons, (d) after the optimization of the atomic coordinates for all atoms. The calculations of (e), (f), and (g) were carried out for single molecules extracted from the crystal structures used for the calculations of (b), (c), and (d).

reproduced. From these results, it is obvious that AP-Ala_3 and P-Ala_3 structure can be clearly distinguished from ^{13}C NMR isotropic chemical shifts.

Figs. 4 and 5 show the experimental ^{15}N NMR spectra and calculated isotropic chemical shifts for AP-Ala_3 and P-Ala_3. Of these, the calculations in Figs. 4 (c) and 5 (c) were in excellent agreement with the experimental results in Figs. 4 (a) and 5 (a), respectively. The difference between the results by GIPAW and GIAO methods is considered to originate from intermolecular packing. The chemical shifts of nitrogen atoms are often affected to hydrogen bonding between adjacent molecules and the formation of hydrogen bonding is closely related to the β-sheet structure. Therefore, details of hydrogen bonding in alanine oligomers may be analyzed by this method.

In conclusion, experimental ^{13}C and ^{15}N NMR spectra of AP-Ala_3 and P-Ala_3 were well reproduced by GIPAW NMR calculation, which have been difficult to reproduce by GIAO method. By using GIPAW calculations, we expect that intermolecular packing can be analyzed precisely from simple solid-state MAS spectra. Now we are working on more detailed analysis, including intermolecular hydrogen bonding, using ^{14}N, ^{1}H and ^{17}O as well as ^{13}C and ^{15}N NMR calculations.

Acknowledgements

This research was supported by a Grant-in-Aid for Scientific Research (23245045). This research was also supported by the Japan Society for the Promotion of Science (JSPS) through its Funding Program for World-Leading Innovative R&D on Science and Technology (FIRST Program). Computation time was also provided by the Super Computer Laboratory, Institute for Chemical Research, Kyoto University.

References

[1] Asakura, T.; Okonogi, M.; Nakazawa, Y.; and Yamauchi, K. *J. Am. Chem. Soc.*, **2006**, *128*, 6231.
[2] Suzuki, Y.; Okonogi, M.; Yamauchi, K.; Kurosu, H.; Tansho, M.; Shimizu, T.; Saito, H; Asakura, T. *J. Phys. Chem.* B **2007**, *111*, 9172.
[3] Yamauchi, K.; Okonogi, M.; Kurosu, H.; Tansho, M.; Gullion, T.; Asakura, T. *J. Magn. Reson.,* **2008**, *190*, 327.
[4] Pickard, C. J.; Mauri, F. *Phys. Rev. B*. **2001**, *63*, 245101.
[5] Suzuki, F.; Kaji, H. *The 49th Annual Meeting of the NMR Society of Japan*, **2010**, 114. ; Suzuki, F.; Kaji, H. *Yuki-EL Tohronkai*, **2010**, *10*, 21.

P-090
Y

Three Dimensional Solid-state NMR study of 7TM-Halorhodopsin

Hajime Tamaki[1], Marika Higuchi[1], Ayako Egawa[2], Masakatsu Kamiya[1], Takashi Kikukawa[1], Tomoyasu Aizawa[1], Keiichi Kawano[1], Toshimichi Fujiwara[2] and Makoto Demura[1]

[1]Graduate School of Life Science, Hokkaido University and
[2]Institute for Protein Research, Osaka University.

ABSTRACT

Halorhodopsin (HR) is a seven-transmembrane (7TM) protein and acts as a light-driven chloride pump in the lipid membrane environment. The purpose of this study is to characterize the structure and dynamics of HR in the lipid environment by solid-state NMR. We report high-resolution 3D spectra for sequential assignment. They are fundamental results of structural and dynamic analysis of HR using solid-state NMR.

Introduction

While membrane proteins constitute approximately a third of all proteins, their high resolution structures are significantly underrepresented in PDB, with only about 200 unique structures known to date. Structural studies of membrane proteins are particularly important because more than half of membrane proteins are drug targets. In recent years, there have been intense efforts to apply structural biology tools, such as X-ray crystallography, electron microscopy, and solution NMR, to membrane proteins, yet it is fair to say that there are still no universal methodologies for preparation of crystals of good quality for X-ray and electron microscopy studies, nor solubilization conditions for solution NMR. Therefore, structural determination of membrane proteins remains one of the biggest challenges in structural biology.

Solid-state NMR (SSNMR) provides ways to study the structure and dynamics of membrane proteins in their lipid environment. It has been increasingly used in recent years to provide accurate structural information in the form of distance constraints, accurate torsional constraints, and orientational constraints for transmembrane helices. The capability of magic-angle spinning (MAS) SSNMR to solve complete protein structures has recently been demonstrated for several small globular proteins in a microcrystalline form. MAS SSNMR study of membrane proteins is more challenging because of its generally lower sensitivity, high spectral degeneracy, and more complicated sample preparation.

We have started SSNMR study of the structure and dynamics of archaeal rhodopsin in the lipid environment. Halorhodopsin (HR), a member of archaeal rhodopsins, is a seven-transmembrane protein. It contains retinal as a chromophore and acts as a light-driven chloride pump in the lipid membrane environment. Its pump activity is related to cellular electrochemical potential. In the photo-excited state or chloride-bound state, HR would undergo dynamic structural changes such as helix moving, opening of uptake channel, etc. However, there is no direct evidence for these structural changes of HR in the lipid. The purpose of this study is to characterize the structure and dynamics of HR in the lipid environment by using SSNMR. In this study, we performed three-dimensional solid-state NMR measurement using uniformly or amino acid reversely ^{13}C and ^{15}N labeled halorhodopsin for the first step.

Membrane Protein, Halorhodopsin

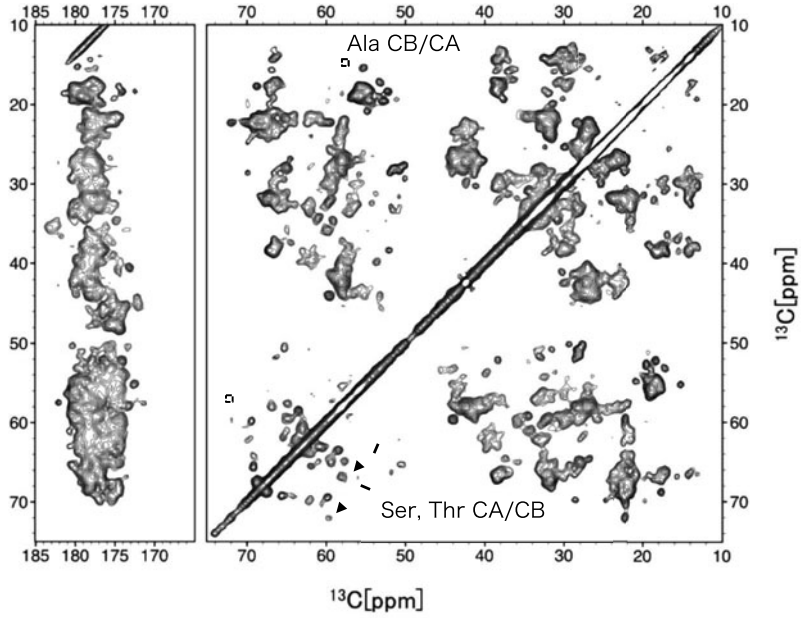

Fig.1 2D ^{13}C-^{13}C Correlation spectrum of uniformly ^{13}C, ^{15}N labeled *Np*HR
Carbon-carbon mixing steps were performed under DARR in 20ms. Downfield shifted serine and threonine peaks are indicated by arrows. Alanine, serine and threonine resonances are shown in the box.

Materials and Methods

E. coli strain BL21 (DE3) cells were transformed with a plasmid encoding C-terminally 6× His-tagged *Natronomonas pharaonis* HR (*Np*HR), and cultured in M9 minimal medium using $^{13}C_6$-glucose and ^{15}N-ammonium chloride. After cells harvesting and breaking by French press, crude membrane was solubilized by n-dodecyl-β-D-maltoside (DDM). The supernatant containing *Np*HR was purified by Ni-NTA-agarose. *Np*HR was reconstituted into liposome, constituted of DMPC-d_{54} and DMPA (9.72:1, w/w) lipid mixture, at a lipid:protein molar ratio of 20:1. Reconstituted *Np*HR was washed several times in 100mM NaCl, 10mM sodium acetate, pH 5.0, and placed in a 3.2-mm o.d. zirconia pencil-type rotor. SSNMR measurements were performed on a Varian Infinity-plus 600 and 700 spectrometer operating at 600 and 700 MHz, respectively. The MAS frequency was kept at 12.5 kHz. The probe temperature was maintained at -5^{o}C. Carbon-carbon mixing steps were performed under DARR.

Results and Discussion

To examine the sample quality, we collected 2D ^{13}C-^{13}C and ^{13}C-^{15}N (NCACX) correlation spectra of uniformly labeled *Np*HR. Downfield shifted serine and threonine peaks (Fig.1, indicated by arrows) strongly suggest *Np*HR in proteoliposome has β-sheet structure. It has been reported that crystal structure of *Np*HR (PDB ID: 3a7k) has short β-sheets in the loop between 2nd and 3rd transmembrane helices called B-C loop, which contains the corresponding residues, serine and threonine. In addition, some serine and threonine residues are contained in the short interhelical loop regions. The results from a ^{13}C-^{13}C correlation experiment agree with the crystal structure. High dispersion of alanine, serine and threonine peaks in the box of Fig.1 and glycine peaks in a NCACX spectrum (data not shown) indicate homogeneous sample condition. We performed three-dimensional solid-state NMR of 3D-NCACX, NCOCX, CONCA for the sequential assignment. As a result, we succeeded in obtaining high-resolution 3D spectra. In addition, we confirmed a sequential backbone walk have been constructed by these 3D spectra.

These results are fundamental of structural and dynamic analysis of 7TM-protein, *Np*HR by using SSNMR.

P-091 A solid-state NMR study of structural alteration and function of the PH domain induced at the lipid bilayer surface.

Naomi Tokuda[1], Katsuhisa Kawai[1], Young-Ho Lee[2], Takahisa Ikegami[2], Hitoshi Yagisawa[1], Yasuhisa Fukui[3] and Satoru Tuzi[1]
[1]Grad. Schl. Life Sci., Univ. Hyogo, Japan,
[2]Inst. for Prot. Res., Osaka Univ., Japan,
[3]Natl. Hlth. Res. Inst., Taiwan

ABSTRACT

In this study, we focus on interaction between the pleckstrin homology (PH) domain and lipid bilayer surface which regulates membrane localization of proteins through recognition of phosphoinositide head-groups. Previously, we reported the conformational transition of the C-terminal α-helix of SWAP-70 PH domain involving nuclear localization signal (NLS) by using circular dichroism (CD) and solid-state NMR spectroscopy. Here, we investigate conformational alteration of NLS-lacking SWAP-70-like adapter of T cells (SLAT/Def6) PH domain. In spite of a high sequence homology of the PH domains of Def6 and SWAP-70, far-UV CD and solid-state NMR spectra show that the C-terminal α-helix in these PH domains adopt different conformations at the lipid bilayer surface.

INTRODUCTION

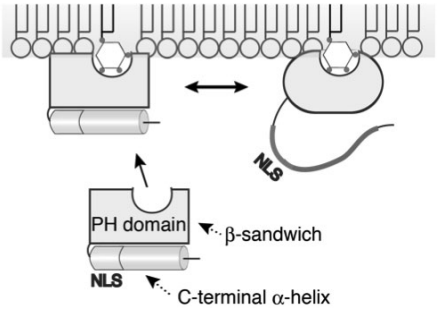

Fig. 1 A model for conformational transition of the SWAP-70 PH domain at the lipid bilayer surface.

The SWAP-70 PH domain has a typical PH domain tertiary structure that consists of a β-sandwich and a C-terminal α-helix located at one of the splayed corner of the β-sandwich in solution. Previously, we reported that the C-terminal α-helix of the SWAP-70 PH domain undergoes α-helix to random coil transition when binds to PIP_3 embedded in vesicles to expose nuclear localization signal (NLS) in the C-terminal α-helix (Fig. 1). Def6 PH domain shares 55% sequence homology with the SWAP-70 PH domain (Fig. 2) but lacks NLS. In this study, we compared the conformation of the Def6 PH domain at the lipid bilayer surface with that of the SWAP-70 PH domain, and discussed in relation to the nuclear localization properties.

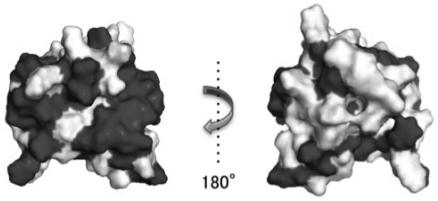

Fig. 2 The model structure of the SWAP-70 PH domain. Homology region between Def6 and SWAP-70 are shown in black.

Keyword: lipid bilayer, PH domain, NLS

RESULT & DISCUSSION

Although the 3D structure of the Def6 PH domain has not been determined, the sequence homology suggests that the structure of the Def6 PH domain is identical to that of the SWAP-70 PH domain. A CD spectrum of the unliganded Def6 PH domain (Fig. 3A, solid line) shows similar characteristics to that of the SWAP-70 PH domain, indicating that the secondary structure of these PH domains in solution is identical. The backbone structure of the Def6 PH domain predicted by TALOS+ from solution NMR spectra also support the structural similarity to the SWAP-70 PH domain. Previously, we reported the α-helix to random coil transition of the C-terminal α-helix of the SWAP-70 PH domain at the membrane surface. This conformational transition causes an increase in negative value of CD at wavelength shorter than 220 nm, characteristics of a random coil structure. As shown in Fig. 3, CD spectrum of the Def6 PH domain is altered when bound to POPC/PIP_3 vesicles (dashed line) indicating a conformational alteration. A decrease in the negative value between 205 and 220 nm reveals, however, that the random coil is not induced at the membrane-bound state. Fig. 5 shows ^{13}C NMR spectra of the [3-^{13}C]Ala-labeled Def6 PH domain. The chemical shift displacements of whole peaks in the spectra of the Def6 PH domain bound to Di-O-DMPC/PIP_3 vesicles (Fig. 5B and C) compared with those in the spectrum of the unliganded-state in solution (Fig. 5A) indicate overall conformational alteration of the PH domain including the C-terminal α-helix (Ala305, Ala306 and Ala310), β-sandwich (Ala234 and Ala294) and loops (Ala264 and Ala286) (Fig. 5B and C). The Def6 PH domain shows significant distortion of the core secondary structure of the PH domain at the lipid bilayer surface, but the α-helix to random coil transition of the C-terminal characteristic of the SWAP-70 PH domain is likely not to be induced. This difference in the structure at the membrane surface seems to be related to a lack of NLS in the Def6 PH domain.

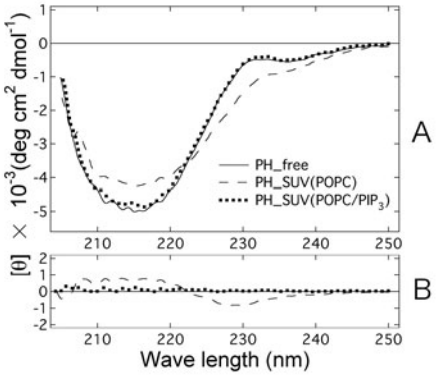

Fig. 3 Far-UV CD spectra of the Def6 PH domain. (A) CD spectra of unliganded PH domain in an aqueous buffer (—) and PH domains bound to the SUV consists of POPC (···) and POPC/PIP_3 (– –). (B) CD difference spectra of PH_SUV(POPC)–PH_free (···) and PH_SUV(POPC/PIP_3)–PH free (– –).

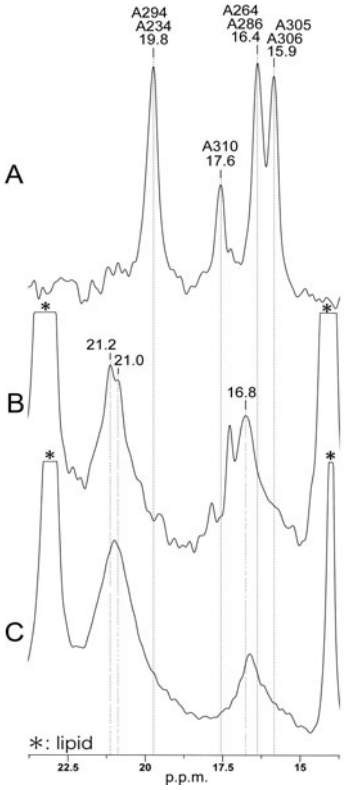

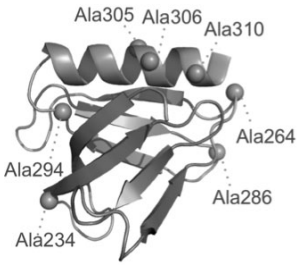

Fig. 4 Position of Ala residues of the Def6 PH domain superimposed on the 3D structure of the SWAP-70 PH domain.

Fig. 5 ^{13}C NMR spectra of [3-^{13}C]Ala-labeled Def6 PH domain. Unliganded PH domain in solution (A), DD-MAS (B) and CP-MAS (C) ^{13}C NMR spectra of the PH domain bound to PIP_3 embedded in Di-O-DMPC/PIP_3 vesicles.

P-092 Photo-induced dynamics change of Phoborhodopsin with transducer as studied by ^{13}C solid-state NMR

Izuru Kawamura[1], Ryutaro Furusato[1], Tetsuro Hidaka[1], Takashi Okitsu[2], Akimori Wada[2], Naoki Kamo[3], Akira Naito[1]

[1]Graduate School of Engineering, Yokohama National University, Japan
[2]Department of Organic Chemistry for Life Science, Kobe Pharmaceutical University, Japan
[3]College of Pharmaceutical Sciences, Matsuyama University, Japan

Abstract

Phoborhodopsin is a photo-receptor and forms a complex with the transducer protein. In this study, we prepared [3-^{13}C]Ala, [20-^{13}C]retinal-labeled *p*pR and simultaneously detected retinal photoisomerization and protein dynamics change of *p*pR with transducer in the lipid environment by *in-situ* photo-irradiated solid-state NMR. In ^{13}C CP-MAS NMR spectra, the signal intensity of C-terminal region in the M-intermediate was decreased compared with that in the dark. This means that dynamics of C-terminal region change to higher fluctuation state in the M-intermediate with activated state of transducer.

Introduction

Pharaonis phoborhodopsin (*p*pR or Sensory rhodopsin II) is a negative phototaxis receptor of *Natronomonas pharaonis* and forms a complex with its cognate transducer protein (*p*HtrII). It is important for signal transduction to investigate the change of protein conformation and dynamics with retinal photoisomerization. In particular, M photo-intermediate during photocycle, which has long lifetime (1.7 s), is thought to be active state for signal transduction. We previously observed ^{13}C NMR signal of [3-^{13}C]Ala-labeled *p*pR at 16.8 ppm of *p*pR C-terminal region and its dynamics change with *p*HtrII using by D75N mutant like M-intermediate [1, 2]. Here, we present *in-situ* photo-irradiation solid-state NMR study of photo-activated *p*pR with *p*HtrII. We report the dynamics change of *p*pR C-terminal region with retinal photoisomerization.

Materials & Methods

[3-^{13}C]Ala-, [1-^{13}C]Val- and [20-^{13}C]retinal-labeled C-terminally histidine-tagged *p*pR was expressed in *E. coli* BL21(DE3) strain on M9 medium containing [3-^{13}C]Ala and [1-^{13}C]Val by addition of 1 mM IPTG and 10 μM [20-^{13}C] all-*trans* retinal. *p*HtrII (1-159) was prepared by using the same method. These proteins were solubilized using n-dodecyl-β-D-maltoside (DDM) and purified with a Ni-NTA agarose, respectively. Purified proteins in DM were reconstituted into egg PC lipids (protein:PC molar ratio of 1:30).

Solid-state ^{13}C NMR spectra were recorded on Chemagnetics CMX-400 infinity FT-NMR spectrometer equipped with *in-situ* photo-irradiation system [3]. ^{13}C CP (cross polarization)-MAS and DD (dipolar decoupling)-MAS with single pulse excitation were performed at -20 and 0°C. In

---

Keyword 1: Solid-state NMR, Keyword 2: dynamics, Keyword 3: Photointermediate

these NMR measurements, to accumulate M-intermediate, we irradiated green laser light (532 nm) to sample.

Results & Discussion

In CP-MAS NMR spectra of [3-^{13}C]Ala-, [1-^{13}C]Val- and [20-^{13}C]retinal-labeled *p*pR with pHtrII (1-159) at MAS 4 kHz, ^{13}C NMR signal of retinal appeared at 13.6 ppm in the ground state of *p*pR and the signal shifted to 22.8 ppm for the M-intermediate at 0°C under photo-irradiated condition. And we observed at least three distinct M-intermediates at -20°C. Furthermore, the yields of overall M-intermediates in *p*pR were evaluated to be 45% and 80% at 0 and -20°C, respectively. Thus, we can successfully and efficiently trap M-intermediate in NMR experiments.

We have assigned NMR peak of [3-^{13}C]Ala-*p*pR at 16.8 ppm to Ala228, 234, 236, 238 located at C-terminal region [1, 2]. In CP-MAS NMR spectra, the signal intensity of C-terminal region in the M-intermediate was obviously decreased by comparison with that in the dark. This means that dynamics of C-terminal region of *p*pR change to higher fluctuation state in the M-intermediate with activated *p*HtrII. Therefore, it is suggested C-terminal region of *p*pR is participated in binding with *p*HtrII at the ground state and this region is released at M-intermediate. This finding is closely consistent with our switch model using D75N mutant with *p*HtrII (1-159) [2] (Figure 1).

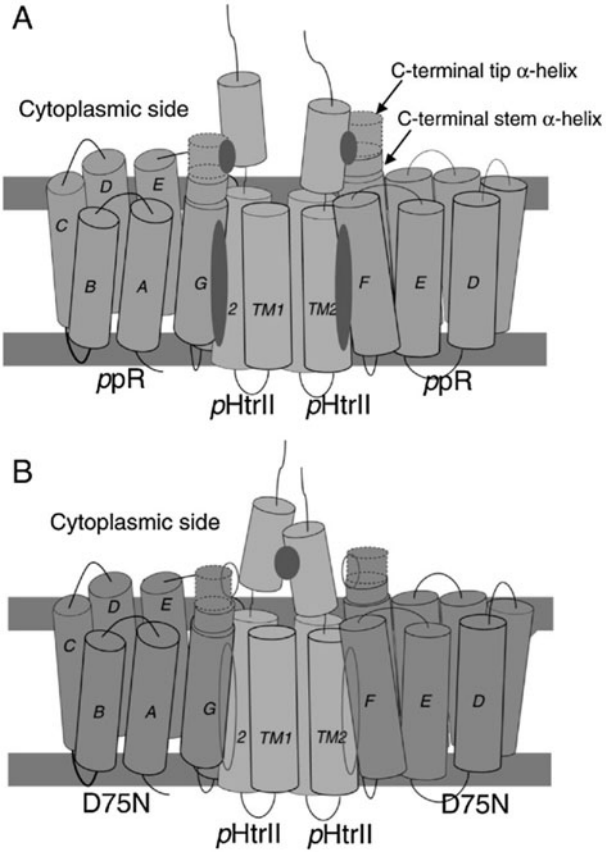

Figure 1. Schematic representation of the interaction of the C-terminal region in *p*pR and D75N with *p*HtrII [2].

In summary, we have successfully detected the M-intermediate form *p*pR with *p*HtrII using *in-situ* photo-irradiated solid-state NMR system. We have shown the dynamics change of C-terminal region with retinal photoisomerization. It is suggested that the dynamics of C-terminal region of *p*pR correlates closely with photo-signaling transduction as well as transmembrane part of helix F and G.

[1] I. Kawamura et al. (2007) *Photochem. Photobiol.* 83 339-345.
[2] I. Kawamura et al. (2008) *Photochem. Photobiol.* 84 921-930.
[3] I. Kawamura et al. (2007) *J. Am. Chem. Soc.* 129 1016-1017.

P-093 Integrated analysis of low-solubility biomass by a combination of NMR and other methods

Hiroshi Hayashi[1], Amiu Shino[2] and Jun Kikuchi[1,2,3,4]

[1]Grad. Sch. of Nanobio., Yokohama City Univ., [2]RIKEN Plant Sci. Cent.,[3]Biomass Eng. Prog., RIKEN, [4]Grad. Sch. of Bioagri., Nagoya Univ.

ABSTRACT

Lignocellulose is the main component in plant biomass, composed of cellulose, hemicellulose and lignin. The lignocellulose bound to form a complex structure is not just mixture of these molecules, but behaves as self-assembled supramolecules. However, its mechanical and physical properties, which contribute to effective use of plant biomass, are still unrevealed. For better understanding of properties, we compared those among grasses and trees by various treatments and instruments. Here, we discussed an analysis based on Solid State NMR and its integrated approach to other properties.

INTRODUCTION

Plant biomass as renewable materials, is mixture and heterogeneous that components are mainly lignocellulose. So it was limited to primitive use. However, recent expectation for green innovation makes attention as feedstock of bio-refinery. But generally, these biomass macromolecules have been studied using isolated state from their mixture components in the past because of its difficulties. This complex mixture which is composed by lignin, cellulose and hemicellulose maintain strongly associated structure. Therefore we need to analyze not only isolated and purified component but also using mixture state. So we analyzed it by using variety of measurement hard ware to know physical properties from micro to macro scale. Then we perform integrated analysis to link their physical properties and chemical structures (Fig.1).

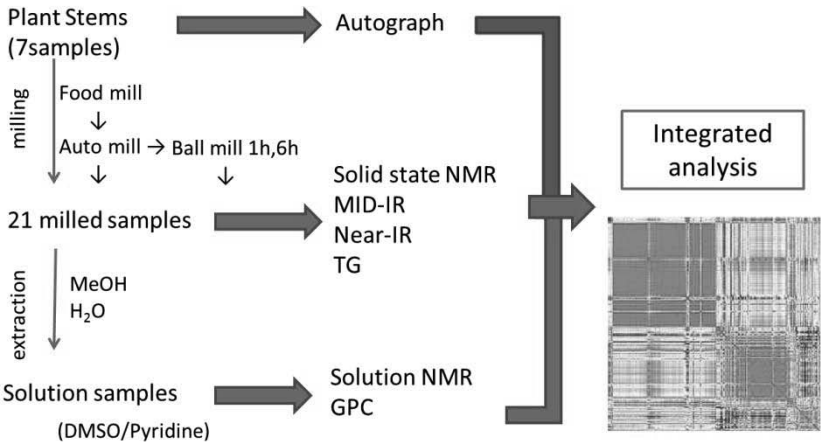

Fig1. Integrated analysis of low solubility biomass

METHODS

We used 4 grasses, 2 broadleaf trees and 1 needle leaf tree as target samples. Then these 7 samples were prosessed by auto-mill, and 2 different conditions by ball-mill. For Solid state NMR experiment, with the aim to know supramolecular structure, CP/MAS experiments was performed using the following experimental parameters. The CP contact times were 1 ms and 5 ms. Magic angle spinning was performed at 12 KHz. In addition, we measured its physical properties by variety of polymer analysis such as IR, TG-DTA, GPC and solution NMR. Then these data integrated analysis by using R and Hetmap (https://database.riken.jp/ecomics/chika/index.html).

Plant biomass, Solid State NMR, Integrated analysis

RESULTS and DISCUSSION

^{13}C Solid state NMR spectra observed some peaks are structural information on lignocellulose composed hemicellulose like xylan, lignin and cellulose (Fig.2). Many structurally difference cellulose peaks which are amorphous cellulose and crystal cellulose overlapped. C4 and C6 amorphous peak (84ppm, 63ppm) of ball-milled samples are larger than that of an auto-milled sample. Crystal cellulose processed by ball-mill changed to amorphous state. In this way, these signals have structural information and cellulose C4 and C6 peaks especially include it. Heatmap of Solid state NMR spectra and Near Infra-Red (NIR) spectra show high correlation of signals from cellulose (fig.2). Thus, we could mine useful information about plant biomass structure to assign complementary with Solid state NMR and NIR spectroscopy. We will discuss further integral approach to other properties during the symposium.

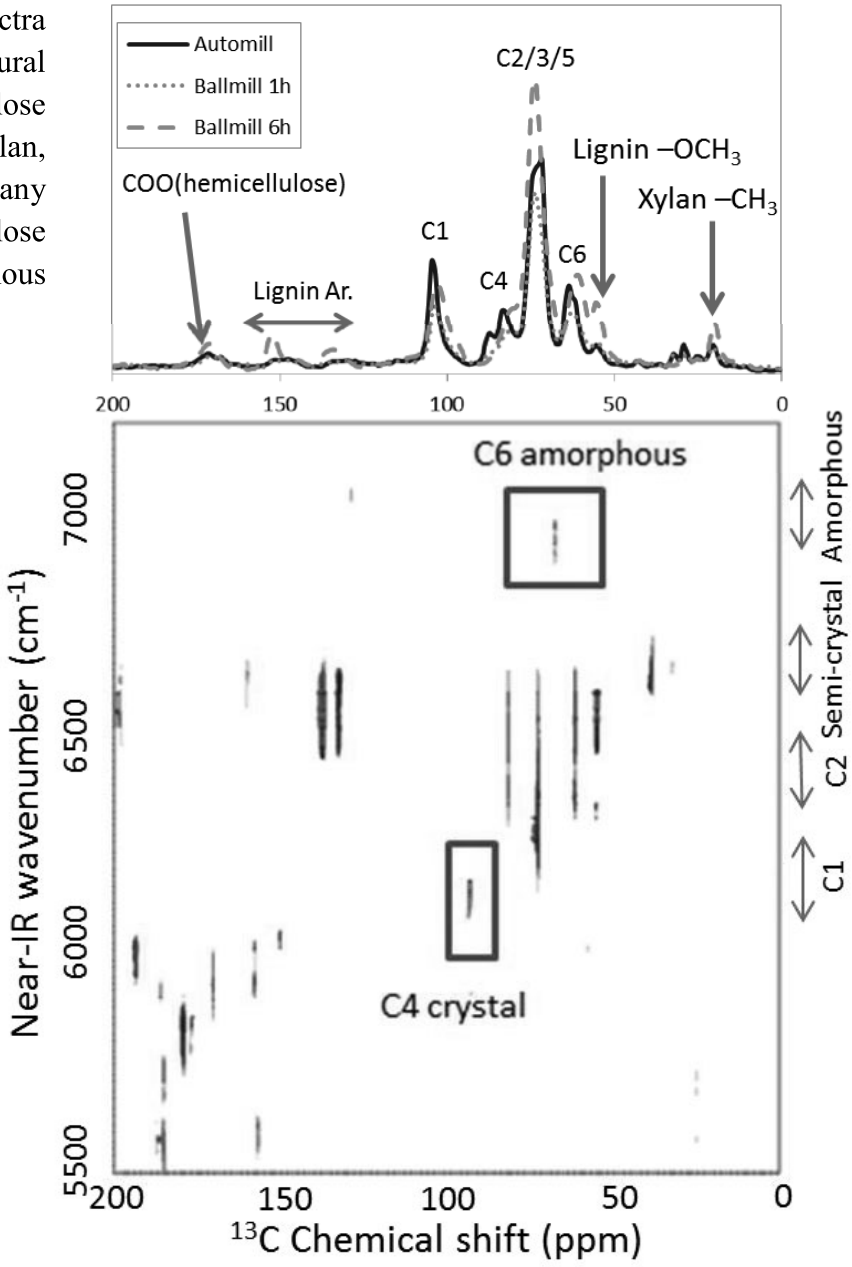

Fig.2. Integrated analysis with solid state NMR and NIR. Top; CP/MAS spectra of differently pretreated nepier grass. Bottom; Heatmap between CP/MAS vs. NIR data.

REFERENCES

1) Kikuchi, J. et.al, *Evaluation of environmental and business significance for unused biomass applications,* Sci&Tech. (2010).
2) Kikuchi, J. et.al, *Braintechnonews*, **124**, 16-21 (2007).
3) Kikuchi, J. *Reg. Plant Growth Dev*, 43, 144-155 (2008).

P-094 Hydrogen-bonding network and rotational motion of Ser side-chain studied by solid-state NMR

Tsunenori Kameda[1], Hidetoshi Teramoto[1], Daisuke Hashizume[2], Hiroyuki Koshino[2], Katsuyuki Nishimura[3]
[1]National Institute of Agrobiological Sciences, Japan
[2]RIKEN Advanced Science Institute, Japan
[3]National Institutes of Natural Sciences, Japan

We clarified the crystal structure of tri-L-serine ($(Ser)_3$) using the synchrotron powder X-ray diffraction (PXDR) analysis. $(Ser)_3$ in the crystalline state is packed in a parallel β-sheet arrangement. The three side chain branches in $(Ser)_3$ are involved in three different types of hydrogen bonding: Side chain 1 bonds with two main chains, while side chain 2 bonds with another side chain; side chain 3 bonds with a side chain and a main chain. From solid-state NMR experiments, it was found that the degree of side-chain rotation differs with the type of hydrogen-bonded structure formed. The variable-temperature ^{13}C CP-MAS NMR spectra for $(Ser)_3$ revealed that line broadenings caused by an interference between the side-chain rotation and ^{1}H decoupling were observed in the temperature range -30–60 °C for side chains 2 and 3. Since the ^{1}H decoupling power used was 81 kHz, the rates of the rotational motions for side chains 2 and 3 were mainly around 10^5 Hz in the relevant temperature range.

1. Introduction: Even when Ser is in the solid state, for example, in peptide crystals and protein fibers, its side chains rotate about the C_α–C_β axis. This side chain rotation is considered to be severely restricted by hydrogen bonding involving the OH group in the side chain.[1] To study the relationship between the formation of hydrogen-bonded structures and the restricted rotation of the Ser side chain, tri-L-serine ($(Ser)_3$) is a suitable compound, because $(Ser)_3$ is a small peptide and each of the three side chains in $(Ser)_3$ may be involved in different types of hydrogen bonding.

Solid-state NMR has emerged as a powerful technique for studying the structure and side-chain dynamics of peptides because of its potential applications in high-resolution techniques. The distinct peaks in the high-resolution solid-state ^{13}C NMR spectrum of a given peptide crystal provide site-specific information about each individual amino acid. Therefore, information about the hydrogen bonding and dynamics of each of the side chains in $(Ser)_3$ can be independently obtained by high-resolution ^{13}C solid-state NMR.

Hydrogen-bonded structure in $(Ser)_3$ crystal has been unknown, because it is difficult to obtain sufficiently large $(Ser)_3$ single crystals for single-crystal X-ray diffraction (XRD) analysis and, thus, no exact geometry of the atoms in $(Ser)_3$ crystal has been given. With the recent development of a technique that combines synchrotron XRD measurements and diffraction pattern simulation, it has become possible to carry out XRD analysis of crystalline powders for atomic structure determination, even when single-crystal samples are not available.

In this study, we clarify the exact geometry of the atoms in $(Ser)_3$ crystal using the combination of synchrotron powder XRD and pattern simulation techniques, then, investigate the relationship between the formation of hydrogen-bonded structures and the restricted rotation of the Ser side chain using solid-state NMR.

Keywords: Serine, Hydrogen bond, Side-chain rotation

2. Experimental: The $(Ser)_3$ sample was purchased from Bachem AG (Bubendorf, Switzerland). ^{13}C and ^{15}N labeled $(Ser)_3$ was manually synthesized. High-resolution 1D and 2D solid-state ^{13}C and ^{15}N NMR spectra were recorded using an Infinity 300 spectrometer (Agilent-Varian-Chemagnetics) and Avance 600 WB (Bruker). The actual sample temperatures were determined from the ^{207}Pb resonance of solid $Pb(NO_3)_2$ used for calibration.

3: Results and Discussion:

Three Ser residues positioned at the N-terminal, center, and C-terminal of $(Ser)_3$ are named as Ser(1), Ser(2), and Ser(3), respectively. The OH groups of the $C_\beta(1)H_2OH$ and $C_\beta(3)H_2OH$ side chains are involved in two types of hydrogen bonding. The OH group of $C_\beta(1)H_2OH$ bonds to $H_3N(1)^+$ and $C'(3)OO^-$ in the main chains of the neighboring molecules; on the other hand, the OH group of $C_\beta(3)H_2OH$ bonds to $C'(3)OO^-$ in the main chain and $C_\beta(2)H_2OH$ in the side chain. The OH group of $C_\beta(2)H_2OH$ bonds only to one side chain of $C_\beta(3)H_2OH$.

As can be seen in Fig. 1, three sharp peaks attributable to $C_\beta(1)$, $C_\beta(2)$, and $C_\beta(3)$ appear at temperatures below –37.8 °C. With a further increase in temperature, the $C_\beta(2)$ and $C_\beta(3)$ peaks broaden and once again become narrow above 70.0 °C. However, no such broadening is observed for the $C_\beta(1)$ peak. The broadening of the $C_\beta(2)$ and $C_\beta(3)$ peaks is attributed to an increase in the segmental motion and the interference between the segmental motion and the ^1H dipolar decoupling. The segmental motion is considered to be the rotation of the side chain about the C_α–C_β axis. Since the ^1H decoupling power used was 81 kHz, the rates of rotational motions for $C_\beta(2)H_2OH$ and $C_\beta(3)H_2OH$ side chains were mainly around 10^5 kHz in the relevant temperature range.

The above-mentioned result that no broadening is observed only for the $C_\beta(1)$ peak is considered to be caused by the restriction on the side-chain rotation due to the hydrogen bonding in the $C_\beta(1)H_2OH$ side chain. This restriction is the strongest among those for the three side chains of $(Ser)_3$. This strong restriction is because the $C_\beta(1)H_2OH$ side chain forms hydrogen bonds with the two main chains. On the other hand, the restrictions on the side-chain rotations are weaker in the case of the other two side chains because these side chains form hydrogen bonds with another side chain. From these results, the relationship between the formation of hydrogen-bonded structures and the restricted rotation of the Ser side chain in a $(Ser)_3$ crystal was found.

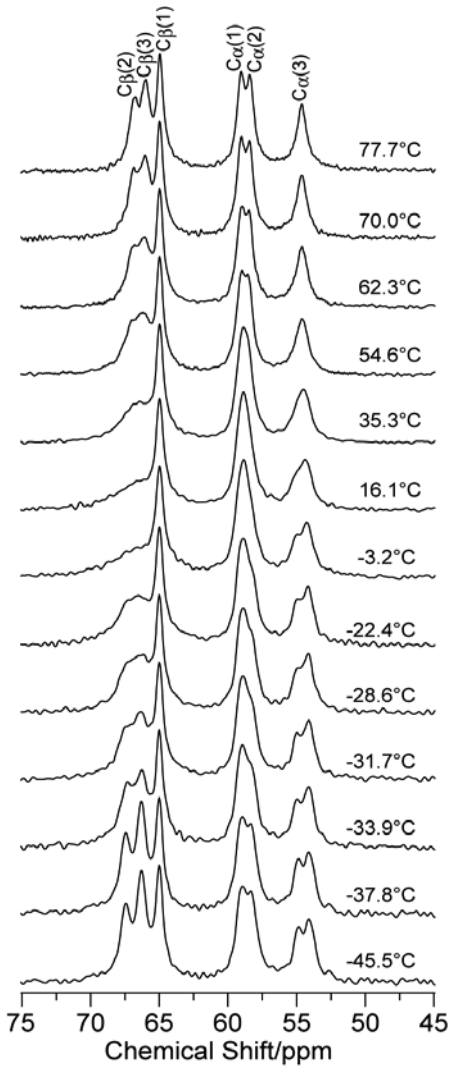

Fig. 1 Expansion of C_α/C_β region in ^{13}C CP/MAS spectra recorded for the $(Ser)_3$ powder at various temperatures.

References

1) Kameda et al., *Macromolecules,* **32**, 7166 (1999).

P-095 Analysis of local dynamics of hydration water in lysozyme crystal using ^{1}H-^{2}H two-dimensional heteronuclear correlation MAS-NMR

Hiroaki Takahata[1], Ryutaro Ohashi[1] and Motohiro Mizuno[1]
[1]Department of Chemistry, Graduate School of Natural Science and Technology, Kanazawa University (Japan)

ABSTRACT
We researched local dynamics of hydration water in lysozyme. In this study, lysozyme with deuterated hydration-water was measured by solid-state two-dimensional proton-deuterium heteronuclear correlation NMR between hydration water and lysozyme. To obtain high-resolution proton spectrum, phase-modulated Lee-Goldburg (PMLG) method was applied. Deuterium slice spectrum about each of proton peaks in obtained two-dimensional spectrum was analyzed by simulation using motional models of hydration-water molecules.

INTRODUCTION

Recently, protein crystals are expected as neo functional materials. It is important for material development to examine the motion of hydration water in protein crystals, because the properties of protein are greatly influenced by the hydration water that surrounds the protein molecules. Our laboratory has researched relation between structures and properties of proteins by analysis of hydration water with ^{2}H NMR. One of those is hen egg white lysozyme. In previous works, it was shown that hydration water of lysozyme crystal have three types of water molecules, 'quasi-static state (static)', '180 degree flip motion (flip)', and 'isotropic rotation (rotation) '. It was also shown that abundance ratios of these types of water are changed by distance between ^{2}H of the hydration water and ^{1}H of the protein. The ratio of the isotropic rotation decreased when the experiments were performed using VACP, in contrast, the ratios of the 'static' and the 'flip' were increased. In this study, local dynamics of hydration water around individual functional-group of lysozyme are analyzed by observing correlation between the deuterated hydration water and the ^{1}H of lysozyme using PMLG [1] technique.

EXPERIMENTAL

Materials: The sample was obtained by the following process. Hen egg white lysozyme, purchased from Wako Pure Chemical Industries, Ltd., was dissolved and recrystallized three times in heavy water. After D_2O absorption, hydration level was 0.21 g water/g protein.

NMR experiments: All NMR experiments were performed on a JEOL ECA-300 spectrometer using a JEOL 4 mm CPMAS probe. Larmor frequencies of ^{1}H and ^{2}H are 295 and 45 MHz, respectively.

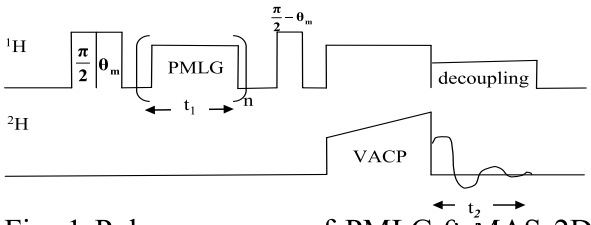

Fig. 1 Pulse sequence of PMLG-9 MAS 2D experiments. θ_m is the magic angle.

hydration water,

^1H – ^2H heteronuclear correlation two-dimensional experiments were carried out using a pulse sequence shown in Fig. 1 with PMLG-9 under MAS at the spinning frequency of 5.0 kHz. Spectral simulations were performed with DMfit [2].

RESLUTS AND DISCUSSION

Two-dimensional spectrum of lysozyme is shown in Fig. 2. In Fig. 2, horizontal and vertical axes represent ^2H offset frequencies and ^1H chemical shifts, respectively. ^1H spectrum under ^1H {PMLG-9} irradiation is shown in Fig. 3. In Fig. 3, peak (1), (2) and (3) are at 2.2 ppm, 4.5 ppm and 8.0 ppm, respectively. The three peaks are assigned as follows; (1) is CH_3 or βCH, (2) is αCH, and (3) is NH or aromatic rings. Fig. 4 shows ^2H spectrum corresponding to ^1H peak (1) in Fig. 3.

Fig. 5 show simulation adjusted to spectrum shown in Fig. 4. The simulation was performed using three components. The spectrum of sum of three components is shown in Fig. 5. Instead of three molecular states, 'static', 'flip', and 'rotation', the three static models, which have the different quadrupole coupling constant (CQ) value, were applied in spectral simulation. In the two static models corresponding to 'flip' and 'rotation', each CQ value is considered as averaged by the each molecular motion. CQ and asymmetry parameter (η) were optimized as follows; (CQ, η) = (205 kHz, 0.2), (41 kHz, 0.0), and (11 kHz, 0.0). It is considered that the component CQ = 205, 41 and 11 kHz correspond to 'static', 'flip', and 'isotropic rotation', respectively. Abundance ratios of the components CQ = 205, 41 and 11 kHz are approximately 89.5, 7.8 and 2.7%, respectively. Most of water molecules around CH_3 or βCH are 'static'. In the remaining, the 'flip' molecules are more than those of 'rotation'. Other ^2H slice spectra will be shown in the poster presentation.

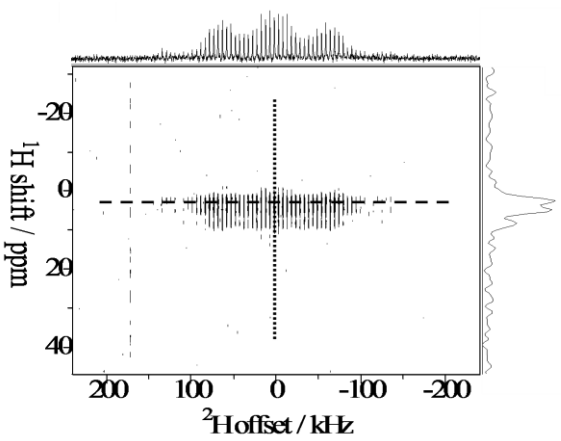

Fig. 2 Two-dimensional PMLG experiment

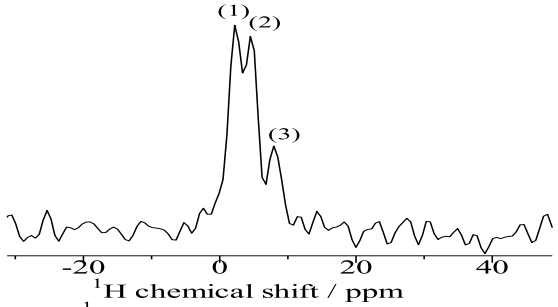

Fig. 3 ^1H slice spectrum of vertical dot-line in Fig. 2. Three peaks are assigned to CH_3 or βCH (1), αCH (2), and NH proton (3).

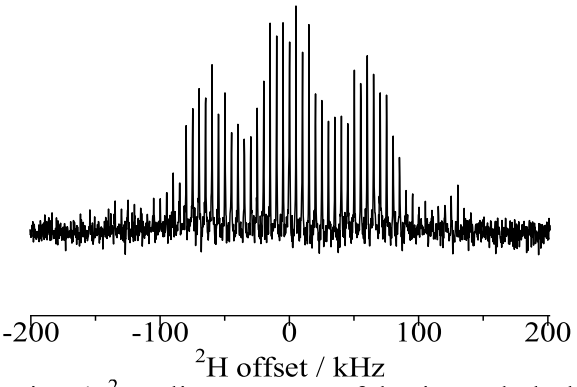

Fig. 4 ^2H slice spectra of horizontal dash line in Fig. 2, and corresponding to peak Fig. 3 (1).

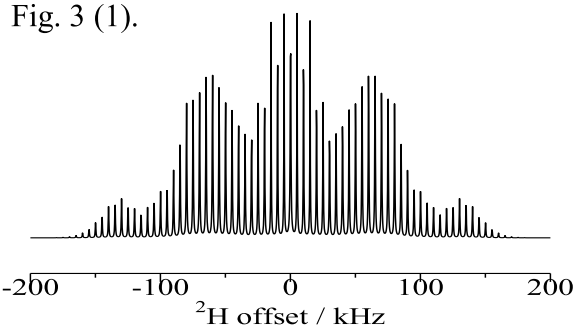

Fig. 5 Simulation spectrum adjusted in Fig. 4

REFERENCE

[1] E. Vinogradov, P. K. Maduhu, S. Vega, Chem. Phys. Lett. 314 (1999) 443.
[2] D. Massiot, F. Fayon, M. Capron, et al, Magn. Reson. Chem. 40 (2002) 70.

P-096 Dynamical analysis of hydrated water in hen egg white lysozyme crystal using solid-state deuterium NMR

Ryutaro Ohashi[1], Hiroaki Takahata[1], Ryo Kaneko[1], Takashi Araya[1], Takao Kazikawa[1], Motohiro Mizuno [1]

[1] Department of Material Chemistry, Natural Science & Technology, Kanazawa University (Japan)

ABSTRACT

Hydration water in protein crystal is one of interesting subjects for material science because it is considered to relate to structure and function of protein. To analyze temperature dependence of correlation between water and protein molecules, lysozyme was recrystallized with deuterium water three times, and the lysozyme crystal was measured with $^{1}H/^{2}H$ Cross Polarization technique at the temperature between 149 K and 301 K. The experimental deuterium spectra were analyzed with simulated quadrupolar powder spectra under molecular motion of water.

INTRODUCTION

Hydration water of protein crystals strongly influences structures and properties of the proteins. Therefore, dynamics analysis of hydration water of protein crystals is essential to understand correlation between structures and properties of proteins.

We have analysed molecular dynamics of hen egg white lysozyme (lysozyme) using solid-state ^{2}H NMR spectroscopy. In the previous study, spectral analysis of ^{2}H Q-echo NMR spectra of D_2O in lysozyme crystals indicated that the lysozyme crystals have three kinds of states of ^{2}H nucleuses. The two states of ^{2}H nucleuses are considered to be in D_2O which have different modes of molecular motion, 180 degree flip motion around C2 axis of D_2O (180-flip) and isotropic rotation (rotation) around each oxygen nuclear. The other state is quasi-static state for ^{2}H NMR spectroscopy. Quasi-static states of ^{2}H nucleuses are considered ^{2}H in slowly-motional D_2O or ^{2}H bonding to lysozyme molecules because some ^{1}H of lysozyme can exchange ^{2}H of D_2O. Moreover, cross polarization (CP) experiments were applied for the lysozyme crystals hydrated D_2O at different hydration levels to obtain information of D_2O close to the lysozyme molecules. These experiments indicated that D_2O molecules of 180-flip have more amount of surrounding ^{1}H nucleuses than other states of ^{2}H.

In this study, to analyse correlation between the hydration levels and ^{2}H motion of D_2O close to the lysozyme molecules, $^{1}H/^{2}H$ CP experiments were done at several temperatures for powder of micro-crystallized lysozyme hydrated D_2O. Moreover, to analyse correlation between ^{1}H motion in the lysozyme and those of ^{2}H motion of D_2O, T_1 measurements of ^{1}H using $^{1}H/^{2}H$ CP technique were examined. These T_1 measurements can extract T_1 relaxation time of ^{1}H close to D_2O.

EXPERIMENTAL

Sample preparation: All samples of lysozyme crystals hydrated D_2O at different hydration-levels were prepared by the following process. Hen egg white lysozyme and D_2O were purchased from Wako Pure Chemical Industries, Ltd. The powder samples of micro-crystallized lysozyme were dissolved and recrystallized in D_2O three times. It is known that ^{1}H of accessible sites in lysozyme

deuterium NMR, crystal water, solid-state NMR

can exchange ^{2}H of hydration heavy water [1]. Hence, most of ^{1}H nucleuses at the accessible sites are considered to be replaced by ^{2}H on three times of recrystallization. After D_2O absorption, hydration levels were adjusted at 0.08 h (g water/g protein) (Dry sample) and 0.26 h (Wet sample). All powder samples were sealed in 6.5 mm glass tubes.

NMR experiments: All NMR experiments were performed for static samples on JEOL ECA-300 spectrometer using Chemagnetics 7.5 mm CPMAS probe. Larmor frequencies of ^{1}H and ^{2}H are 295 and 45 MHz, respectively.

RESULTS AND DISCUSSION

$^{1}H/^{2}H$ CP spectra of Dry and Wet sample at the temperatures from 149 K to 301 K. In both of Dry and Wet sample, the line-shapes show characterized powder patterns of ^{2}H nucleuses from quasi-static state (pake-pattern at outside of the line-shapes) and 180-flip state (arch shapes at center of the line-shapes) of ^{2}H nucleuses. The line-widths of center signals from 180-flip are decreasing in rising temperature. It indicates that 180-flip at low temperature is slower than at high temperature. The ratios of signals assigned 180-flip and quasi-static states are not apparently changed at all temperatures. Hence, D_2O molecules close to lysozyme molecules are considered to be hardly influenced. The intensities of center signals assigned 180-flip of Wet sample are larger than those of Dry sample at all temperatures. It indicates that since quasi-static ^{2}H close to ^{1}H of lysozyme are bonding to accessible sites of lysozyme, signal intensities of quasi-static ^{2}H were not changed in both of Dry and Wet sample. In contrast to quasi-static states, signal intensities of 180-flip ^{2}H in Wet sample were larger than those in Dry sample because 180-flip ^{2}H nucleuses belong to hydrated D_2O.

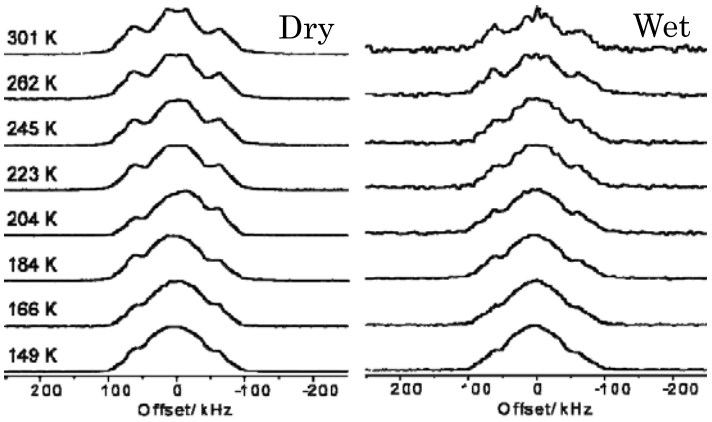

Fig. 1 $^{1}H/^{2}H$ CP spectra of Dry and Wet sample.

To compare with CP spectra in Fig. 2, Q-echo spectra of Dry and Wet sample are shown in Fig. 3. In Fig. 3, the line-shapes of Wet sample are quite different from those of Dry sample because of sharp signals assigned isotropic-rotation states. It is considered that CP experiments extracted spectra of ^{2}H close to ^{1}H of lysozyme. Since isotropic rotation reduces dipole-dipole interaction, the position of rotation ^{2}H cannot be known in this study. Analysis using spectral simulation and T_1 relaxation will be shown in the poster presentation.

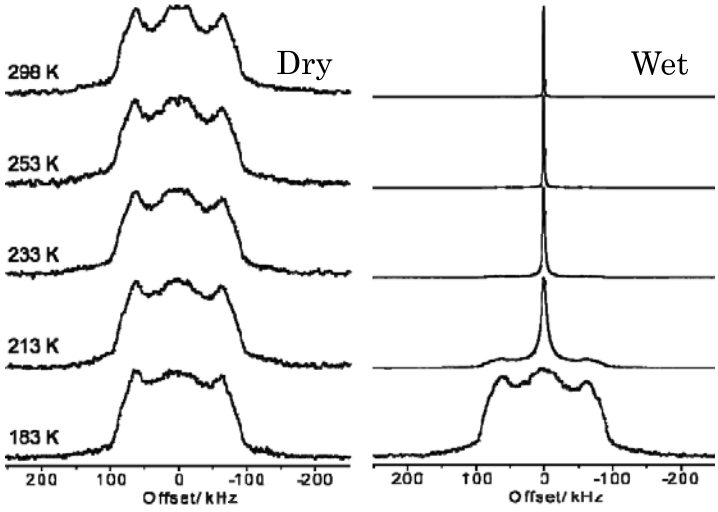

Fig. 2 ^{2}H Q-echo spectra of Dry and Wet sample.

[1] O.B.Peersen, X. Wu, I. Kustanovich, S.O.Smith, J. Magn. Reson., A104, 334 (1993).

P-097
Y

Strain Induced ^{13}C Chemical Shift Change of Natural Rubber after MAS

Masashi Kitamura, Atsushi Asano, Chikako T. Nakazawa and Takuzo Kurotsu
Department of Applied Chemistry, National Defense Academy

ABSTRACT

For elastomers, deformation caused by fast MAS occurs during measuring NMR spectra. We found that the deformation (strain) of elastomers induces ^{13}C chemical shift (CS) change for static measurements, while the ^{13}C CS change does not occur under the MAS conditions. For natural rubbers without vulcanization, the ^{13}C CS changes with the degree of strain and thickness. The ^{13}C CS change observed for very thin NR was explained by the molecular orientation according to the previous study by Kimura, *et al*. on Polymer Journal 2010, **42**, 25-30. However, the ^{13}C CS change detected at relatively thick NR could not be expressed by the orientation. We assumed magnetic susceptibility differences to interpret the interesting phenomenon. To clarify this hypothesis, we have also examined the other rubbers, polyisobutylene and polybutadiene.

INTRODUCTION

We know that elastomers are deformed under fast MAS, but do not know how the deformation (strain) of elastomers affects their ^{13}C chemical shift and molecular motion. Therefore, it is very important to reveal the influence of the deformation by MAS on the molecular motion and chemical shift. In this study, we have investigated the relationship between the degree of extension and ^{13}C chemical shift for NR. We have also investigated the molecular orientation of NR depending on its thickness. Furthermore, we will also discuss the results of polyisobutylene and polybutadiene.

EXPERIMENTAL PROCEDURE

NR of grade RSS#1 was used. Polyisobutylene was purchased from Sigma-Aldrich and polybutadiene was provided by ZEON corporation. Static and solid state ^{13}C NMR measurements were made using a Varian NMR systems spectrometer operating at 100.57 MHz with the 6.0 mmϕ rotor at 30°C. ^{1}H decoupling power was 48 kHz to 68 kHz. NR was rolled by 9 kHz MAS at 60°C with Teflon spacers of various length to control the elongation of NR from 3.4 mm to ca. 20 mm (Figure 1).

RESULTS and DISCUSSION

Figure 1 shows the solid state ^{13}C NMR spectra of NR with and without MAS. Before MAS, isotropic peaks are observed even though under static condition (a). After MAS with Teflon spacer, the static ^{13}C NMR spectrum becomes anisotropic (b). This is because NR is rolled and its shape becomes like a doughnut. After MAS without

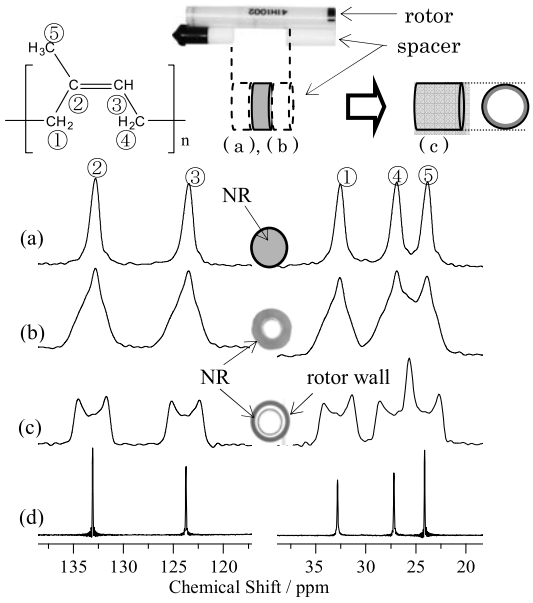

Figure 1 Observed solid state ^{13}C NMR spectra of NR. (a) static before MAS, (b) and (c) static after MAS, (d) MAS spectrum.

Keywords: solid state NMR, natural rubber, MAS, molecular orientation

Teflon spacer, the spectrum shows characteristic peaks like a pake doublet (c). ^{13}C DDMAS NMR spectrum shows very narrow peaks regardless of NR deformation (d). These observations imply that NR molecules are oriented during MAS. The centrifugal pressure of MAS makes NR molecules to be oriented with rolling and stretch. To investigate the direction of molecular orientation, we observed the angular dependent ^{13}C NMR spectra of a short strip of NR, which is cut along the length or circumference directions of rotor, against the static field.

Figure 2 shows the angular dependent ^{13}C NMR spectra of a short strip of NR for both directions. The quarternary ^{13}C NMR peak appears at 134.4 ppm for a strip of NR cut along the length direction of rotor, when the NR is set in the bottom situation against the static field (hereafter, we refer this condition to Bottom). At the Left, the ^{13}C NMR peak is observed at 132.0 ppm. The ^{13}C NMR peak at the Right appears at the same chemical shift with that at the Left. This sequential ^{13}C chemical shift change suggests that molecular orientation occurred for the NR rolled by MAS. By comparing with Kimura's results, we concluded that the molecular axis of NR is oriented to the circumferential direction of the rotor. If the molecular orientation is identical to the circumferential direction of rotor, ^{13}C NMR peak of a strip of NR cut along the circumference direction will not show the angular dependence. In fact, Figure 2 (B) does not show angular dependence. Therefore, it is confirmed that the direction of the orientation is the same with the circumference direction.

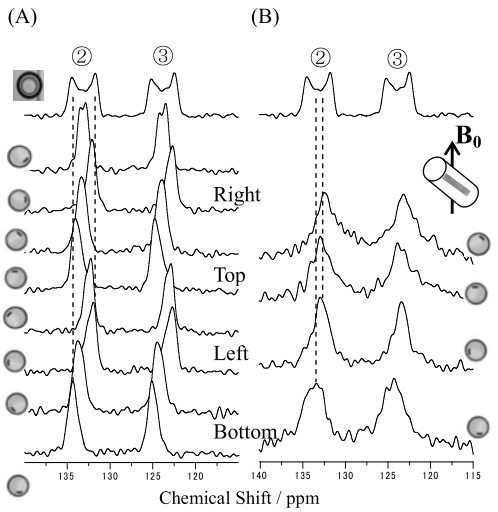

Figure 2 Observed angular dependent ^{13}C NMR spectra of a strip of NR at various angle against the static field. (A) The length direction of rotor. (B) The circumferential direction.

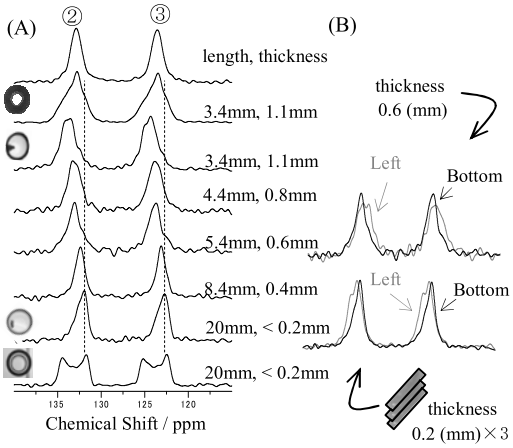

Figure 3 Observed angular dependent ^{13}C NMR spectra of NR rolled at various strain ratio (A). Spectrum at Left is compared to that at Bottom (B).

With increase of elongation ratio (strain) of NR by controlling the length of Teflon spacer during MAS, the angular dependent ^{13}C NMR peak of a strip of NR at the Left shifts from 134 ppm to 132 ppm gradually. If the chemical shift is determined by orientation only, the ^{13}C chemical shift would not alter. In addition, the ^{13}C NMR chemical shift at the Left for NR at 0.6 mm thickness shows similar value with that of Bottom. Superposed three NR strips at ca. 0.2 mm thickness also shows similar tendency with the results of NR at 0.6 mm thickness. This clearly indicates that thickness also contributes to the change of ^{13}C chemical shit. This may be explained by magnetic susceptibility caused by π electrons of double bond in NR. In order to prove this hypothesis, we measured angular dependent ^{13}C NMR spectra of polyisobutylene and polybutene. We would like to discuss them at young poster session on the day.

P-098
Y

Solid-state NMR for polymer thin film devices

Toshiki Obata and Naoki Asakawa*
Department of Chemistry and Chemical Biology
Graduate School of Engineering, Gunma University

ABSTRACT

We describe our results concerning *ex-situ* NMR experiments for thin films under static electric field (EF) or magnetic field gradient (MFG), which are applicable to various samples including organic electronics devices, polymer thin films, etc. First, we performed proton NMR experiments under static EF for the Alminum(Al) / poly(dimethylsiloxane) [PDMS] / Al type sandwiched sample. Next, we succeeded in one-dimensional proton magnetic resonance imaging (MRI) for multilayer thin films of poly(tetrafluoro ethylene) [PTFE] / PDMS / PTFE using the static MFG by a neodymium permanent magnet.

Introduction

Polymer materials had not been used for active electronic device materials mainly because many polymers show unstable electric properties due to poor heat resistance or heat deflection, large structural fluctuation, or chemical instability. Of course, recent developments in organic light emitting diodes(OLED), organic orphotovoltaic cells(OPV), and organic field effect transistors(OFET) have been remarkable, and these applications related to polymers will form a mainstream of polymer electronics. Even so, unstable properties, or more correctly large time and/or spatial fluctuations of physical properties, e.g., carrier mobility and electric conductivity, can be an important determinant in producing noise-driven bio-inspired future electronics devices that we are interested in.

Recently, we have shown the existence of thermodynamic and nonequilibrium twist transitions in regioregulated poly(3-alkyl thiophene)s. Since it has theoretically been predicted that static and dynamic disorder affect the carrier mobility of π-conjugatd polymers, the dynamics associated with the transition could be the origin of random electric properties and would have the potential to be utilized for a stochastic neuromorphic device or a molecular noise generator, which are useful to noise-driven sensing, signal transmission, and information processing with ultra low energy consumption. However, the correlation between molecular dynamics and electric properties are ill-established and developments on methodologies to access the problem have been highly desired for a long time.

In this background, we are interested in probing local spectral density functions of molecular dynamics of π-conjugated polymer devices under their operating conditions. In this poster presentation, we report our attempts on NMR measurements for polymer thin film device elements

Keywords: polymer devices, electric field, relaxation time, magnetic field gradient, MRI

under electric field application and also on NMR micro-imaging measurement under a static magnetic field gradient using a neodymium permanent magnet.

Experimental

We built an *ex situ* variable frequency ^{1}H NMR probe that enables us to perform NMR experiments of samples with tailored shapes such as polymer devices. We tried to make ^{1}H NMR measurements for poly(dimethyl siloxane)[PDMS] film(thickness:200μm) under the static electric field condition. Next, we tried one-dimensional MRI of three layered film (PDMS (thickness:200μm) / PTFE(400μm) / PDMS(200μm)) under the static magnetic field gradient of <100 T/m using small neodymium magnet bar. ^{1}H two-pulse Hahn echo (TPHE) and quadrature echo(QE) methods were used in order to verify whether the measurements were performed under the large MFG. All the measurements were performed using home-built NMR/NQR spectrometer based on a RF pulse generator (SpinCore PulseBlaster DDS-III, SpinCore Tech., Inc.).

Results and discussion

Fig.1 shows the ^{1}H NMR spectra of a Al/PDMS/Al device element under the static electric field. The highest sensitivity on ^{1}H NMR was achieved with the sample setup that the normal vector of Al electrodes should be perpendicular both to B_0 and B_1. This is probably because eddy current which RF pulse causes at Al electrodes' plane is minimized under the condition. From the spectra, we observed inhomogeneous and increase of line width under the condition of V = 60 V(E =3.0 x 10^5 V/m). The broadening of the spectral line could be due to mobile impurities in PDMS .

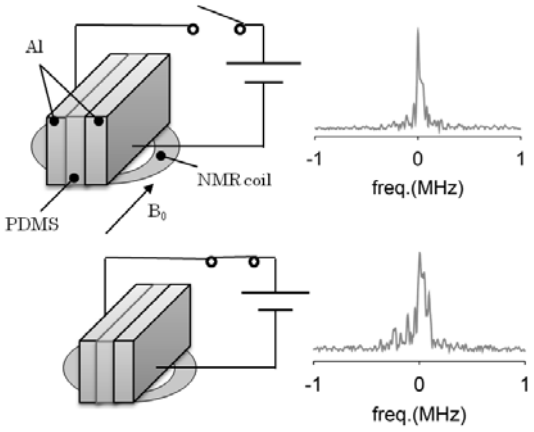

Fig.1 ^{1}H NMR spin-echo spectra for the Al/PDMS/Al device element: V=0V(top) and 60V(bottom).

Next, Fig.2 shows one-dimensional ^{1}H MRI for a PDMS/PTFE/PDMS multilayer film under a static MFG. We found that the QE spectrum was qualitatively different from the TPHE one;that is, the oscillation with large amplitude was visible in the QE spectrum, inferring that the measuments were successfully performed under strong magnetic field gradient. Therefore, we succeeded in inexpensive MRI using a small forromagnet.

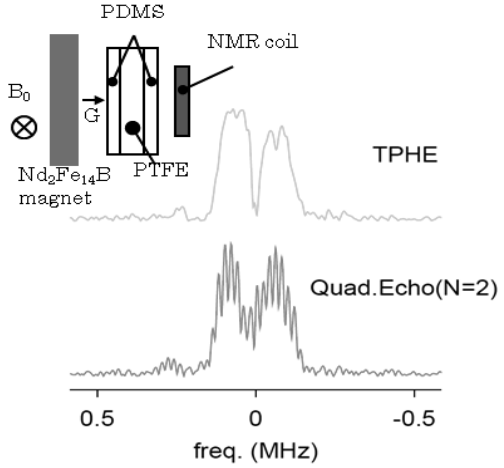

Fig.2 One-dimensional MRI for PDMS/PTFE/PDMS multilayer films.

Finaly, we developed an *ex situ* NMR probe for organic device elements under versatile environment such as electric field and magnetic field gradient. The method would be useful not only to conventional organic device fabrication but also noise-driven sensors and information processors.

P-099 Crystallization mechanism of poly(nonamethylene terephthalamide) as studied by solid state NMR

Keisuke Sunaga, Hiroki Uehara and Takeshi Yamanobe
Department of Chemistry and Chemical Biology, Gunma University

Introduction

Poly(nonamethyleneterephthalamide) (PA9T) is condensation products of terephthalic acid and C9 diamine. PA9T is thermoplastic resin and applied to the connector parts and so on. PA9T has the melting temperature higher than 300°C and its crystallization behavior is not investigated in detail. In this study, crystallization mechanism, structure and molecular mobility of PA9T are discussed by solid state NMR in combination with XRD and DSC.

Experimental

PA9T used in this study is supplied by KURARAY CO., LTD. The crystallized samples are prepared in DSC (Perkin Elmer Diamond DSC). PA9T is melted at 350°C for 10 min. and then cooled to the crystallization temperature (290-320°C). Crystallizations are carried out at each crystallization temperature for 10 min, 1,6,12 and 24 hours. After the crystallization, samples are cooled at the cooling rate of 100°C/min. DSC measurements are carried out in N_2 atmosphere between 50-350°C at the heating rate of 10°C/min. Solid state NMR measurements are carried out by Bruker AVANCE III DSX300WB NMR spectroscopy. Samples are contained in 4mm sample tube and spun at about 5.5kHz.

Results and Discussions

In Fig.1 is shown DSC thermograms for crystallized PA9T at various crystallization temperature for 6 hours. For PA9Ts crystallized at 290 and 295°C, there are three peaks at about290, 305 and 315°C. Heating rate dependent DSC results indicate that the peak at 315°C decreases as the heating rate becomes faster, which means that peak at 315°C corresponds to the melt of the rearranged crystallites produced during heating in DSC. Since peak positions and strength of two thermograms are similar to each other, crystallization at 290 and 295°C corresponds to quench from melt. Crystallizations at 300 and

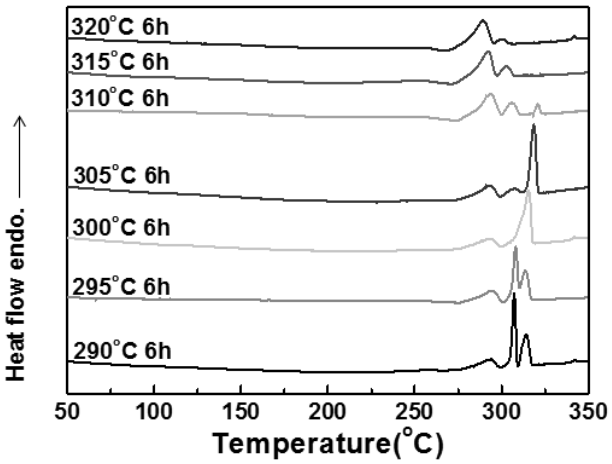

Fig.1 DSC thermograms for PA9T crystallized at various temperatures for 6 hours.

poly(nonamethyleneterephthalamide), PA9T, crystallization, solid state NMR

305°C result in different thermal behavior from those at lower temperature. The strongest melting peak appears at about 320°C, which is higher than those of lower crystallization temperature. Since the peak position moves to higher temperature as the crystallization temperature increases, crystallization proceeds and development of lamellae takes place under these conditions. As the melting peak at about 290°C is independent of crystallization temperature, this peak corresponds to unstable crystallite produced during cooling from crystallization temperature. DSC themgrams for PA9T crystallized at higher than 310°C is completely different from those at lower temperature. The strongest melting peak at about280°C moves to lower temperature as crystallization temperature increases and there is a small peak at about 325°C also. In order to investigate the structure of these crystallized PA9T samples, solid state NMR and X ray are used.

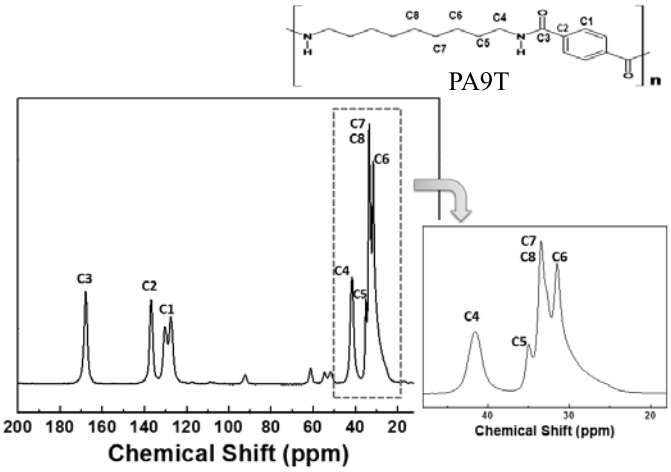

Fig.2 ^{13}C NMR spectrum and peak assignment for PA9T crystallized at various temperatures for 6 hours.

In Fig.2 is shown ^{13}C CPMAS NMR spectrum of initial powder of PA9T. Carbonyl carbon appears at about 170ppm. Although there are two chemically distinct carbons in phenyl, there are three phenyl peaks. This arises from the angle between phenyl and amide planes. CH_2 carbons appear at 20-43 ppm. C4 and C5 appear at lower field because of amide group. Internal methylene carbons, C6,7 and 8, appear at about 31 ppm which is close to the crystalline component of polyethylene. In addition, there is broad component below 30 ppm. This component corresponds to the amorphous component of polyethylene.

^{13}C NMR spectrum of PA9T crystallized for 6 hours is almost independent of the crystallization temperature up to 305°C. Chemical shift of internal methylene is 33ppm which means the internal methylene carbon takes trans zigzag conformation. As splitting of C1 carbon in phenyl is clearest for 305°C crystallized sample, the crystalline phase is most homogeneous of all samples. As the crystallization temperature increased higher than 310°C, the amorphous component of methylene carbon increased. In addition, broadening of phenyl peak is also observed. Increment of the amorphous component means increment of the gausch conformation of methylene part, which indicates the disorder rich state of methylene part. The broadening of phenyl carbon, especially in C1, indicates the broad distribution of dihedral angle for C3-C2 bond. These facts means that the crystallization at higher than 310°C does not proceed efficiently. Static and dynamic structure will be discussed in the presentation.

P-100 Formation of Carbamates and Cross-linking of Microbial Poly(ε-L-lysine) Studied by ^{13}C and ^{15}N Solid-State NMR

Shiro Maeda[1], Ken Takagi[1], Shota Kaneko[1], and Ko-Ki Kunimoto[2]
[1]Division of Applied Chemistry and Biotechnology, Graduate School of Engineering, University of Fukui, Bunkyo, Fukui 910-8507, Japan
[2]Division of Material Engineering, Graduate School of Natural Science and Technology, Kanazawa University, Kakuma-machi, Kanazawa 920-1192, Japan

ABSTRACT Formation of carbamates by amino groups of poly(ε-L-lysine) (ε-PL) and cross-linking of ε-PL were studied by using ^{13}C and ^{15}N solid-state NMR. It is a characteristic found in ε-PL cast from basic aqueous solution exposed to the air or gaseous CO_2. It is not observed in ε-PL cast from acidic aqueous solution and ε-PL cast from degassed aqueous solution under CO_2 free environment. The carboxyl carbon and amide nitrogen appear at 164 ppm in ^{13}C spectrum and 92 ppm in ^{15}N spectrum, respectively, which arise when some amino groups of ε-PL react with gaseous CO_2 to make carbamates. In addition to these peaks a peak at 171 ppm appears. We assigned it to amide C=O carbons which can not make intermolecular hydrogen bondings since there exist bulky carbamates groups close to these C=O groups. Self-assembly of ionic pairs of ammonium groups and carbamate anions leads to cross-linking of ε-PL.

INTRODUCTION

Poly(ε-L-lysine) (ε-PL) (Scheme 1) is one of a few poly(amino acid)s which are known to occur in nature. We have studied the molecular structure and the conformation of ε-PL in aqueous solution. The pH dependent IR, circular dichroism, and ^{1}H solution NMR spectra have indicated that ε-PL assumes a β-sheet conformation in basic aqueous solution and an electrostatically expanded conformation in acidic aqueous solution. It is conceivable that the four methylene groups in the backbone of ε-PL endow the polymer with considerable conformational flexibility compared to the case of poly(α-L-lysine) (α-PL). We have also characterized the structure and the conformation of ε-PL and its derivatives in the solid-state by ^{13}C and ^{15}N solid-state NMR [1-5]. A conformational model of e-PL was also proposed in which the main chain takes a parallel β-sheet similar to the γ-form of nylon 6 [3].

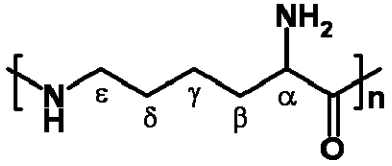

Scheme 1. Repeating units of poly(ε-L-lysine) (ε-PL).

Chemically modified derivatives of ε-PL, ε-PL/MO and ε-PL/DC were prepared through reactions of ε-PL with methyl orange (MO) and dabsyl chloride (DC), respectively. In ε-PL/MO, side chain α-amino groups of ε-PL are involved in ionic bonds with methyl orange (MO) to form poly-ion complexes, (ε-PL)-$NH_3^+SO_3^-$-(MO). On the other hand, ε-PL is reacted with dabsyl chloride in ε-PL/DC to form covalent sulfonamide bonds, (ε-PL)-NH-SO_2-(DC). These chemically modified ε-PL's exhibit ^{15}N NMR signals characteristic of the binding mode at the α-amino groups [5]. Semi-transparent and water soluble films are formed by casting aqueous solution of ε-PL. In this work, we have prepared films cast from aqueous solution of ε-PL at various pH's. ^{13}C and ^{15}N CPMAS NMR spectra were measured and discussed in comparison with those of the ε-PL powder data. In order to confirm the carbamate formation, the measurements were done for films prepared under the degassed and the CO_2 bubbling conditions. [6]

Microbial Polymer, Poly(ε-L-lysine), Solid-state NMR.

EXPERIMENTAL

Materials

Microbial ε-PL (free form, ε-PL) was kindly supplied by Chisso Corporation, Japan. The number-averaged molecular weight of ε-PL was determined to be 4,090, which corresponds to the degree of polymerization of 32 based on the unit molecular weight of 128. Ultra pure water, prepared by a Milli-QPlus ultra-pure water system (Millipore, USA) was used throughout the experiment.

Preparation of ε-PL film cast from aqueous solution

Cast films of ε-PL was prepared as follows: 3.5 wt% ε-PL aqueous solution (pH 9.3) was cast on a Teflon petri dish, dried in the air for four days, and subsequently dried in vacuum for four days at room temperature. The pH of ε-PL aqueous solution was adjusted by adding a small amount of 1 M HCl aqueous solution. The ε-PL film cast from degassed aqueous solution (CO_2 free ε-PL) was prepared as follows: 2 wt% ε-PL solution dissolved in degassed water was cast on a Teflon petri dish under CO_2 free environment and dried in vacuum for two days. ε-PL cast from aqueous solution with CO_2 bubbling (CO_2 bubbling ε-PL) was prepared as follows: CO_2 gas (from dry ice) was bubbled gently through a stirred 2 wt% ε-PL aqueous solution in a glass vial for 6 hours at room temperature. This solution (pH 6.3) was cast on a Teflon petri dish and dried in vacuum for two days.

NMR Measurements

^{13}C and ^{15}N CPMAS NMR spectra were measured with Chemagnetics CMX Infinity 300 operating at 75.6 MHz and 30.0 MHz, respectively, at room temperature. The samples of a cast film cut into small pieces with scissors or in powder form were contained in a cylindrical rotor of zirconia ceramic. The rotor diameter was 5mm, and the rotor was spun at 5.0 kHz or 7.0 kHz. Contact time was 1ms, and repetition time was 1 sec. The number of accumulation was about 2,000 for ^{13}C and about 40,000 for ^{15}N. ^{13}C signal of methyl carbon was externally referenced to 17.35 ppm from tetramethylsilane. ^{15}N signal of glycine was externally referenced to 32.5 ppm from ammonia (liq. NH_3, 25ºC).

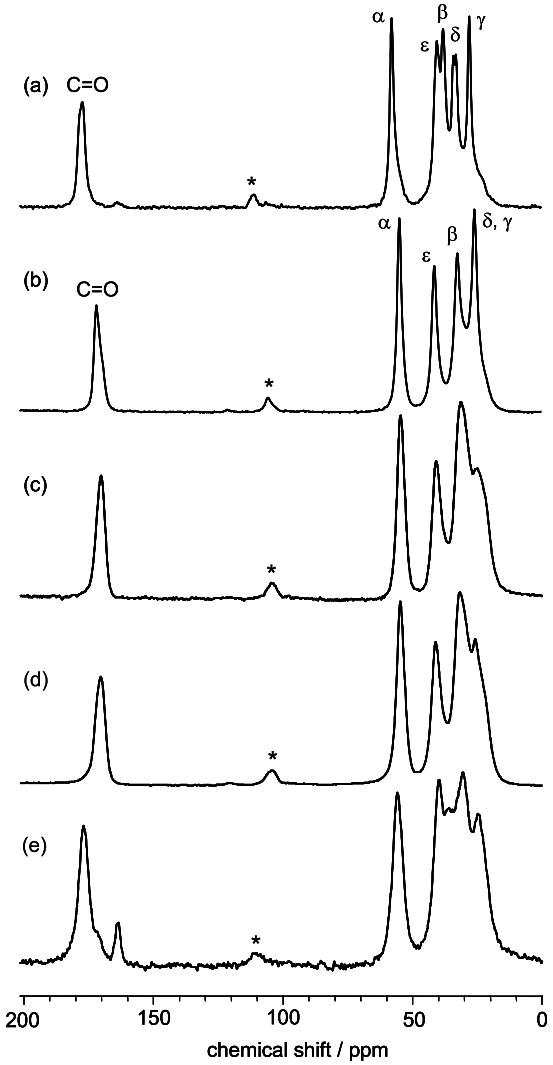

Figure 1. ^{13}C CPMAS NMR spectra of (a) ε-PL powder, (b) ε-PL/HCl powder, and ε-PL film cast from aqueous solution of (c) pH 2.8, (d) pH 4.8, and (e) pH 9.3, respectively. A peak marked with an asterisk is a spinning side-band.[6]

Table 1. ^{13}C chemical shifts of ε-PL and its derivatives in the solid state[a].[6]

Sample	ε-NHCO		α-NHCO	Cα
ε-PL[b]	178.6,177.1			57.0
ε-PL/HCl[b]		171.1		54.9
ε-PL/BOC[b]		171.8		55.3
ε-PL/MO[b]		172.2		55.1
CO_2 free ε-PL	177.6			57.8
ε-PL Cast film	176.5	170.9	163.7	55.7
CO_2 bubbling ε-PL	176.8	171.4	163.7	56.1

a) In ppm with respect to tetramethylsilane.
b) From reference [5].
c)A quaternary carbon signal of BOC (*t*-butoxycarbonyl) appears at 79.4 ppm.

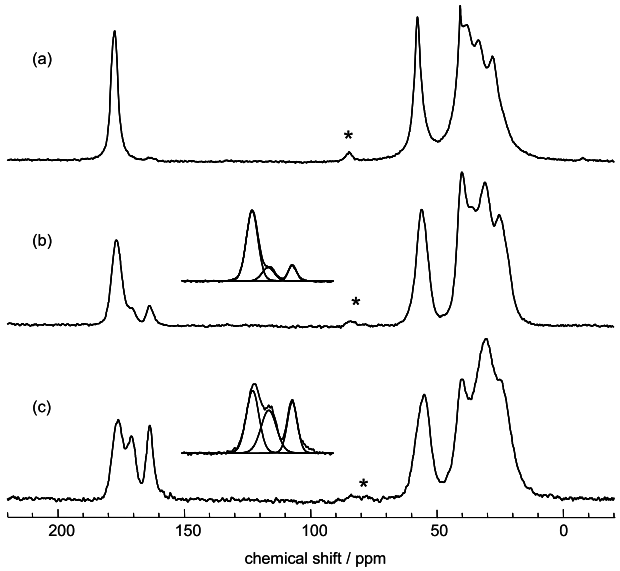

Figure 2. ^{13}C CPMAS NMR spectra of ε-PL. (a) CO_2 free ε-PL, (b) ε-PL cast film and (c) CO_2 bubbling ε-PL. A peak marked with an asterisk is a spinning side-band. Curve-fittings for C=O resonances are shown in the insets.[6]

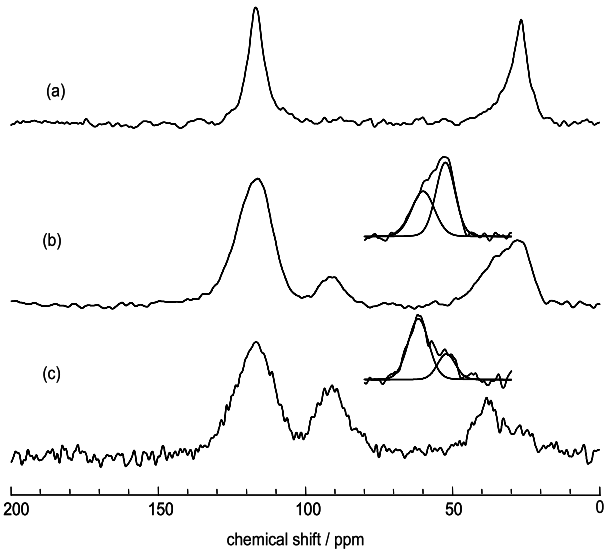

Figure 3. ^{15}N CPMAS NMR spectra of ε-PL. (a) CO_2 free ε-PL, (b) ε-PL cast film, and (c) CO_2 bubbling ε-PL. Curve-fittings for amino groups are shown in the insets.[6]

RESULTS AND DISCUSSION

Figure 1 shows the ^{13}C CPMAS NMR spectra of the ε-PL films cast from aqueous solution at various pHs along with the spectra of powder samples as a reference. As shown in Figure 1(e), the ε-PL film cast from basic aqueous solution shows a small peak at 164 ppm with a shoulder at 171 ppm, in addition to a main peak at 177 ppm. The latter main peak corresponds to the C=O carbon peak of the ε-PL (Fig. 1(a)) [3]. The former peaks at 164 and 171 ppm are not observed in the spectra of the ε-PL films cast from acidic aqueous solution (Figure 1(c) and 1(d)). These samples show a single peak at 171 ppm where C=O peak of ε-PL/HCL powder appears [5]. Table 1 summarizes ^{13}C chemical shifts of NHCO carbons and Cα for ε-PL and its chemically modified derivatives, ε-PL/HCl, ε-PL/BOC (*t*-butoxycarbonyl), ε-PL/MO, CO_2 free ε-PL, ε-PL cast film, and CO_2 bubbling ε-PL. ε-PL/BOC is listed as a reference compound, which is a completely N_α-substituted ε-PL derivative. ε-PL/MO (Methyl Orange) is also listed as a reference compound, which makes poly-ionic complex [5].

Figure 2 compares ^{13}C CPMAS NMR spectra of three types of ε-PL films: (a) CO_2 free ε-PL, (b) ε-PL cast film, and (c) CO_2 bubbling ε-PL. ^{15}N CPMAS NMR spectra of the same samples are shown in Figure 3. The CO_2 free ε-PL film prepared under CO_2 free environment shows only a single peak of C=O at 177.6 ppm. In contrast, the CO_2 bubbling ε-PL and the ε-PL cast film show C=O peaks at 164 and 171 ppm, in addition to large C=O peak at 176.5 and 176.8 ppm, respectively. We attributed the peak observed at 164 ppm in the ε-PL cast film (Figure 2(b)) and the CO_2 bubbling ε-PL film (Figure 2(c)) to the carbonyl carbon of carbamates. The peak at 171 ppm can be attributed to the amide C=O carbon adjacent to the carbamated α-amino group. Bulky carbamate groups close to the amide C=O groups prevent formation of intermolecular hydrogen bonds and destruction of hydrogen bondings caused upfield shifts. The curve fitting results (insets of Figure 2) show that relative intensity ratio of peaks at 178, 171, and 164 ppm are 46, 27, and 27% for CO_2 bubbling ε-PL, and 78, 11, and 11% for ε-PL cast film, respectively. Thus, relative intensity ratio of peak at 178 and 171 ppm are 63 and 37% for CO_2 bubbling ε-PL, and 87 and 13% for ε-PL cast film. The present result indicates that 13% of amino groups of ε-PL forms. Figure 3

shows ^{15}N CPMAS NMR spectra of (a) CO_2 free ε-PL, (b) ε-PL cast film, and (c) CO_2 bubbling ε-PL. Table 2 summarizes ^{15}N chemical shifts of ε-PL, ε-PL/HCl, ε-PL derivatives, CO_2 free ε-PL, CO_2 bubbling ε-PL, and ε-PL cast film.

Table 2. ^{15}N chemical shifts of ε-PL and its derivatives in the solid state[a]. [6]

Sample	ε-NHCO	α-NHCO	α-NH_3^+		α-NH_2
			free	ion-complex	
ε-PL[b]	117				27
ε-PL/HCl[b]	123		44		
ε-PL/BOC[b]	120	92			
ε-PL/MO[b]	115			34	
CO_2 free ε-PL	118				27[c]
ε-PL cast film	116	92		34[c]	27[c]
CO_2 bubbling ε-PL	120	91		38[c]	27[c]

a) In ppm with respect to liquid NH_3 at 25°C.
b) From reference [5].
c) Obtained from curve fitting

We assigned peaks at about 92 ppm in Figure 3(b) and 3(c) to side chain amide nitrogen of carbamates. ^{15}N chemical shifts of CO_2 free ε-PL (Figure 3(a)) are the same as those of ε-PL powder. This fact implies that side chain α-amino groups are not protonated. In contrast spectra of CO_2 bubbling ε-PL and ε-PL cast film show broad peak at about 34 ppm. We reported that side chain α-amino groups of ε-PL in ε-PL/MO are involved in ionic bonds with MO to form poly-ionic complexes [5]. The curve fitting results for α-amino groups of CO_2 bubbling ε-PL and ε-PL cast film (insets of Figure 3) show that the peaks are consisted of two peaks at about 27 and about 34 ppm. We attributed the former peak to nonprotonated amino groups and the latter to protonated amino groups which are involved in ionic bonds with carbamate anion to form poly-ionic complexes. A similar formation of carbamates was recently observed for α-PL.

Figure 4 shows a schematic diagram of structure of partially cross-linked ε-PL due to formation of carbamates.[6] Characterization of ε-PL cast from aqueous solution and dynamics of formation of carbamates are currently studied and will be published in subsequent papers.

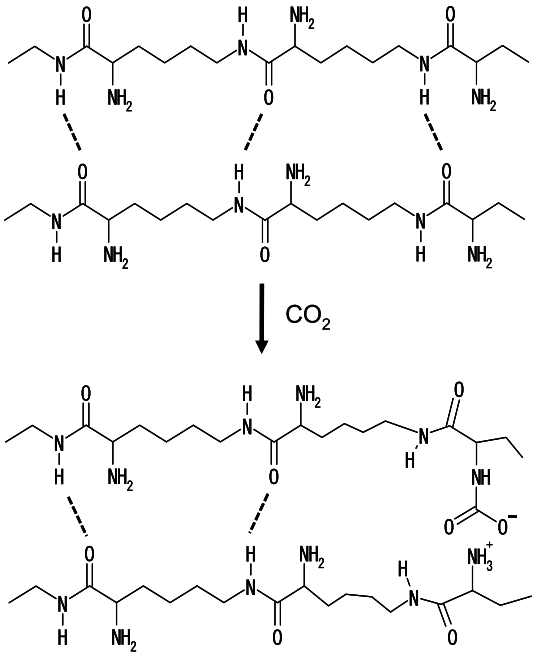

Figure 4. Schematic diagram of structure of partially cross-linked ε-PL due to formation of carbamates. Broken lines show intermolecular hydrogen bondings. [6]

REFERENCES

1. S. Maeda, C. Sasaki, and K.-K. Kunimoto, In: *NMR spectroscopy of polymers: Innovative NMR strategies for complex macromolecular systems. ACS symposium series, American Chemical Society,* in press (2011).
2. S. Maeda, T. Mori, K.-K. Kunimoto, and C. Sasaki, *Kobunshi Kako,* **52**, 516-522 (2003)
3. S. Maeda and K.-K. Kunimoto, *Chemical Engineering*, **56**, 719-724 (Kagaku Kogyosha, Inc., Japan) (2011).
4. S. Maeda, K.-K. Kunimoto, C. Sasaki, A. Kuwae, and K. Hanai, *J. Mol. Struct*., **655**, 149-155 (2003)
5. S. Maeda, T. Mori, C. Sasaki, K.-K. Kunimoto, A. Kuwae, and K. Hanai, *Polym. Bull.,* **53,** 259-267 (2005).
6. S. Maeda, S. Oumae, S. Kaneko, and K.-K. Kunimoto, *Polym. Bull*., in press (2011).